PHYSICAL REVIEW D **86,** 105017 (2012)

Effective matrix model for deconfinement in pure gauge theories

Adrian Dumitru[*]
Department of Natural Sciences, Baruch College, 17 Lexington Avenue, New York, New York 10010, USA and RIKEN BNL Research Center, Brookhaven National Laboratory, Upton, New York 11973, USA

Yun Guo[†]
Department of Physics, Guangxi Normal University, Guilin 541004, China

Yoshimasa Hidaka[‡]
Quantum Hadron Physics Laboratory, RIKEN Nishina Center, Saitama 351-0198, Japan

Chris P. Korthals Altes[§]
Centre Physique Théorique au CNRS Case 907, Campus de Luminy F-13288 Marseille, France and NIKHEF Theory Group, Science Park 105, 1098 XG Amsterdam, The Netherlands

Robert D. Pisarski[‖]
Department of Physics, Brookhaven National Laboratory, Upton, New York 11973, USA and RIKEN BNL Research Center, Brookhaven National Laboratory, Upton, New York 11973, USA

(Received 2 May 2012; published 8 November 2012)

We construct matrix models for the deconfining phase transition in $SU(N)$ gauge theories, without dynamical quarks, at a nonzero temperature T. We generalize models with zero and one free parameter to study a model with two free parameters: besides perturbative terms $\sim T^4$, we introduce terms $\sim T^2$ and $\sim T^0$. The two N-dependent parameters are determined by fitting to data from numerical simulations on the lattice for the pressure, including the latent heat. Good agreement is found for the pressure in the semi quark gluon plasma, which is the region from T_c, the critical temperature, to about $\sim 4T_c$. Above $\sim 1.2T_c$, the pressure is a sum of a perturbative term, $\sim + T^4$, and a simple nonperturbative term, essentially just a constant times $\sim - T_c^2 T^2$. For the pressure, the details of the matrix model only enter within a very narrow window, from T_c to $\sim 1.2T_c$, whose width does not change significantly with N. Without further adjustment, the model also agrees well with lattice data for the 't Hooft loop. This is notable, because in contrast to the pressure, the 't Hooft loop is sensitive to the details of the matrix model over the entire semi quark gluon plasma. For the (renormalized) Polyakov loop, though, our results disagree sharply with those from the lattice. Matrix models provide a natural and generic explanation for why the deconfining phase transition in $SU(N)$ gauge theories is of first order not just for three, but also for four or more, colors. Lastly, we consider gauge theories where there is no strict order parameter for deconfinement, such as for a $G(2)$ gauge group. To agree with lattice measurements, in the $G(2)$ matrix model, it is essential to add terms that generate complete eigenvalue repulsion in the confining phase.

DOI: 10.1103/PhysRevD.86.105017 PACS numbers: 12.38.Mh, 11.15.Ha, 11.10.Wx

I. INTRODUCTION

Quantum chromodynamics (QCD) is a theory of great beauty. Only a handful of input parameters uniquely define its behavior at all distance scales. For the *pure* glue theory, with no dynamical quarks, there is only a single parameter, which sets the overall scale of length.

Conversely, with so few parameters, it is difficult to compute from first principles. A useful technique is to perform numerical simulations on the lattice. While at present simulations with dynamical quarks are extremely challenging, in the pure glue theory results close to the continuum limit can be obtained.

The behavior of gauge theories at a nonzero temperature, T, is of particular interest. There are lattice results for the thermodynamic behavior of pure $SU(N)$ gauge theories [1,2] for two [3], three [4–7], and four or more colors [8–13]. They show that in the pure glue theory, the thermodynamics for small N is like that for large N. The lattice results find a pressure, $p(T)$, which is small in the confined phase, below the critical temperature, T_c. Scaled by the pressure of an ideal gas of gluons, the ratio $p(T)/p_{\text{ideal}}(T)$ grows sharply in the range from T_c to about $4.0T_c$ and is then approximately constant above $T > 4T_c$; $p/p_{\text{ideal}} \sim 0.85$ at $4T_c$. We term the region over which the pressure grows markedly, from T_c to $\sim 4.0T_c$, as the

[*]dumitru@quark.phy.bnl.gov
[†]yun@fias.uni-frankfurt.de
[‡]hidaka@riken.jp
[§]chrisaltes@gmail.com
[‖]pisarski@bnl.gov

 © 2012 American Physical Society

semi quark gluon plasma (semi-QGP) [14,15]; see, also Refs. [16–19].

At large N, the sharp increase in the pressure at T_c is elementary. In the confined phase there are only colorless glueballs, so the pressure is small, ~ 1. In the deconfined phase, the pressure is proportional to the number of gluons, $= N^2 - 1 \sim N^2$, and so large. Lattice simulations for three [4,5] and even two colors [3] also find that the pressure below T_c is much smaller than that above.

The similarity between small and large N can be made quantitative. To parametrize the deviations from ideality, consider the conformal anomaly, which is the energy density, $e(T)$, minus three times the pressure. Dividing by the number of gluons, lattice studies show that as a function of T/T_c, the dimensionless ratio $(e - 3p)/((N^2 - 1)T^4)$ is similar for $N = 3$, 4 and 6 [11,12]: above $T > 1.2T_c$, this ratio falls with increasing T.

Since the order of the transition changes with N, this similarity breaks down close to the transition, below $1.2T_c$. The deconfining transition is of second order for two colors [3], weakly first order for three [4,5], and first order for all $N \geq 4$ [9,11,12]. While the ratio of the latent heat to the number of gluons is a number of order one as $N \to \infty$, this ratio increases significantly as N does [9,12].

In this paper we use these detailed results from the lattice to develop an effective theory for deconfinement in the pure glue theory. A common model for deconfinement is to take a term like that of an ideal gas minus a MIT bag constant, B: $p(T) \sim c_1 T^4 - B$. If true, then above $\sim 1.2T_c$, the conformal anomaly/T^4 would fall off as $\sim B/T^4$.

To understand the falloff, consider the following quantity [7,11,12,14,20–23]:

$$\tilde{\Delta}(T) = \frac{e(T) - 3p(T)}{(N^2 - 1)T_c^2 T^2}. \tag{1}$$

That is, we plot the conformal anomaly divided not by T^4 but by T^2 times T_c^2 to form something dimensionless. We also divide by the number of perturbative gluons to be able to compare different numbers of colors. If a bag constant dominated, this quantity would fall off at large T as $\tilde{\Delta}(T) \sim B/(T_c^2 T^2)$.

For three colors, there is precise data from the WHOT Collaboration [6]. We show $\tilde{\Delta}(T)$, extracted from the WHOT data, in Fig. 1. Between 1.2 and $2.0T_c$, this ratio is constant to $\sim 1\%$. This implies that in this range, the pressure can be approximated as

$$\begin{aligned} p(T) &\approx c_1(T^4 - c_2 T_c^2 T^2); \\ c_2 &\approx 1.00 \pm 0.01; \qquad T/T_c\text{: } 1.2 \to 2.0. \end{aligned} \tag{2}$$

There is no data from Ref. [6] above $2.0T_c$.

There are recent results over a broad range of temperature from Borsanyi *et al.* [7]. They find that from 1.3 to $4.0T_c$, $\tilde{\Delta}(T)$ is constant to within $\sim 5\%$, Fig. 6 of Ref. [7].

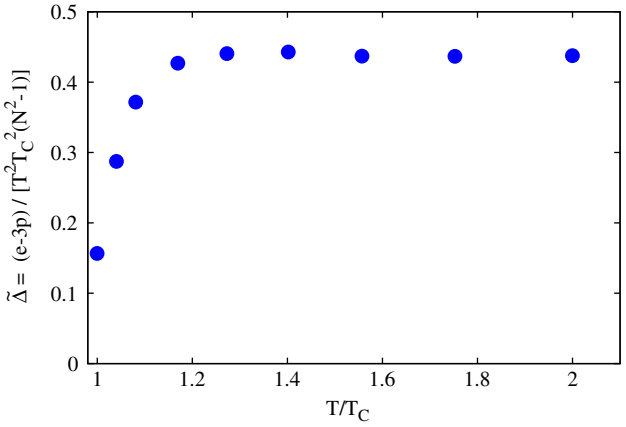

FIG. 1 (color online). Plot of the trace anomaly divided by T^2, $(e - 3p)/(8T^2T_c^2)$, from the data of Umeda *et al.*, Ref. [6]; see also Borsanyi *et al.*, Ref. [7].

At much higher temperature, $\tilde{\Delta}(T)$ grows because of the running of the coupling constant, Fig. 10 of Ref. [7].

The same constancy is also seen for four and six colors, albeit with larger error bars [11,12]. Notably, the width of the window in which $\tilde{\Delta}(T)$ is constant does *not* appear to change significantly as the number of colors increases from $N = 3$ to $N = 4$ or 6 [11,12]. This indicates that the narrow width of the window is not a large N effect, which vanishes as $N \to \infty$.

The fact that nonideal terms in the pressure are $\sim T^2$ was first noted in Ref. [20] and then later in Ref. [21]; see also the discussions in Refs. [7,14,22,23]. One implication, used previously by us in Ref. [14] and also here, is that since the ideal gas term is T^4, any nonperturbative terms that we introduce are assumed to be proportional only to even powers of T, such as $\sim T^2$, $\sim T^0$, *etc.*

Less obviously, with hindsight many features of our model can be understood from Fig. 1. We use a $SU(N)$ matrix model, where the basic variables are the eigenvalues of the thermal Wilson line. The vacuum at a temperature T is given by varying an effective Lagrangian with respect to these N matrix variables, the q's; the pressure is (minus) the value of the potential at this minimum. Even without knowing what the q's are, though, clearly the simplest way of obtaining a constant term $\sim T^2$ in the pressure is simply to introduce a similar constant in the potential for the q's.

This implies that over most of the semi-QGP, above 1.2, to $\sim 4.0T_c$, the decrease of the pressure, relative to that of an ideal gluon gas, is dominated by a *trivial* term, a pure number times $\sim -T_c^2 T^2$. In the deconfined phase, there is a nontrivial minimum of the effective theory, in which the q's are nonzero, only in a surprisingly narrow window, for $T \leq 1.2T_c$.

This is not generic to matrix models but is forced upon us by the lattice data [4–6,9,11,12]. A matrix model for deconfinement was first introduced by Meisinger *et al.* [20]. This model has no free parameters and, as we show

later, a much broader result for $(e - 3p)/T^4$ than seen by the lattice. In Ref. [14] we introduced a model with one free parameter, which allowed us to fit the narrow result for the conformal anomaly observed on the lattice. In the present work we show that agreement with the lattice data near T_c, in particular for the latent heat, requires a two-parameter model.

Ignoring such details, the fundamental question remains: what is the origin of this constant term in the pressure, $\sim -T_c^2 T^2$, which dominates the corrections to nonideality above $\sim 1.2 T_c$?

One natural guess is a gluon *mass* $\sim T_c$. Such a mass is typical, for example, in solutions to the Schwinger-Dyson equations of QCD [24]. After all, if we expand the pressure of massive gas about the massless limit, when $m \ll T$ the leading correction is $\sim -m^2 T^2$.

However, there is no simple form for the mass that will give such a flat result for the rescaled conformal anomaly of Eq. (1). If we take $m \sim T$, then it is not difficult to see that the ideal pressure of such a massive gas is a pure number times T^4. If we take m to have a constant mass, proportional to T_c, then numerically one can check that the only way to obtain a correction $\sim T^2$ is for small masses, $m \ll T_c$; but the value of c_2 in Eq. (2) requires that m is a number of order one times T_c. The only way to fit the pressure is if the gluon mass is an involved function of T. This is what is done in quasiparticle models [25–28]; see, e.g., Eq. (27) of Ref. [27], where their $m(T)$ involves three parameters. In contrast, in a matrix model we can fit the pressure, with a similar accuracy, with one free parameter, the constant $\sim -T_c^2 T^2$.

It is also useful to note that for $SU(N)$ gauge theories in $2 + 1$ dimensions [29,30], the pressure has a similar form to that in Eq. (2). From Fig. 6 of Caselle *et al.* [30], above temperatures of $\sim 1.25 T_c$ the pressure is approximately $p(T) \approx T^3 - T_c T^2$. That is, the nonideal term is *again* $\sim T^2$; this is not a mass term, since in $2 + 1$ dimensions this would be linear in the temperature, $\sim m^2 T$.

Thus the term $\sim -T_c^2 T^2$ in the pressure does not appear to be just a gluon mass. Nor do we know why the window, from T_c to $1.2 T_c$, is so narrow. One might guess that it is an effect $\sim 1/N^2$, but to fit the lattice data, our model requires that the window has about the same width for four and six colors as it does for three. A term $\sim T^2$ is like the free energy of massless fields in two dimensions, such as strings, but how can strings contribute to the free energy, $\sim N^2$, in the deconfined phase?

With our matrix model we also predict features which are not usually addressed by other effective theories. Taking the parameters from the fit to the pressure, we compute the 't Hooft loop in the semi-QGP and find good agreement with lattice data. In contrast to the pressure, for the 't Hooft loop we find that the effects of *nonideal* terms matter not just below $1.2 T_c$ but over the *entire* semi-QGP, from T_c to $\sim 4.0 T_c$. For this reason, the computation of the 't Hooft loop is a sensitive and crucial test of our model.

There is one glaring discrepancy, though, between the lattice data and our model. In our model the Polyakov loop only differs from one when the matrix q's are nonzero, below $1.2 T_c$. This is very different from the behavior of the renormalized Polyakov loop from the lattice [31,32], which varies over the entire semi-QGP. Perhaps the renormalized Polyakov loop does not accurately reflect changes in the eigenvalue distribution. The eigenvalues of the Wilson line can be measured directly in lattice simulations [33,34]. We comment on this further in the Conclusions, Sec. IX.

Matrix models can help give further insight into deconfinement. For $SU(N)$ theories without dynamical quarks, the existence a global $Z(N)$ symmetry gives a rigorous definition for the deconfining phase transition; it implies that the confined phase is necessarily $Z(N)$ symmetric. In a $SU(N)$ matrix model, the confined phase is uniquely characterized by the complete repulsion of eigenvalues. The structure of this point in the space of eigenvalues, which is the Weyl group, is such that the $Z(N)$ symmetry of the confined phase is automatic.

Svetitsky and Yaffe showed that for three colors, the deconfining transition is generally of first order [35]. This is because for three colors, the $Z(3)$ symmetry allows one to form a cubic invariant of Polyakov loops. As is typical of mean-field theory, such a cubic invariant ensures that the transition is of first order. For four or more colors, though, $Z(N)$-invariant terms are of quartic or higher order, and there is no prediction. Note that this assumes that the relevant variables are Polyakov loops, which are elements of the Lie group.

As discussed above, though, lattice simulations show that the deconfining transition is of first order not just for three but for four or more colors. This is explained naturally by matrix models. In expanding our matrix model about the confining vacuum, we find a cubic invariant for any $N \geq 3$. This result is not special to the parameters of our model: we show how if we expand a general matrix model about the point of complete eigenvalue repulsion, then there is a cubic invariant. The presence of a cubic invariant, now in terms of elements of the Lie algebra, instead of the Lie group, implies that the deconfining phase transition is of first order not just for $N = 3$ but for $N \geq 4$.

The details of the transition in our simple matrix model appear to agree with results from the lattice. In particular, while the latent heat (scaled appropriately by $N^2 - 1$) grows from $N = 3$ to large N, the order-disorder interface tension, at T_c, is rather small for all N. In our model this is because there is a potential with a small barrier between two vacua which are relatively far apart.

We also extend our analysis to include other gauge groups. A particularly interesting example is provided by

the exceptional group $G(2)$ [36–41]. This group has a trivial center, so there is no order parameter for deconfinement. Nevertheless, lattice simulations find that there is a strongly first-order phase transition between a deconfined phase at high temperature and a low-temperature phase in which the expectation values of Polyakov loops are very small. That is, although there is no center symmetry, the low-temperature phase still appears to confine.

We do not find that the simplest matrix model reproduces the lattice data for a $G(2)$ gauge group. However, we show how to add terms in the effective matrix model to ensure that the expectation value of Polyakov loops is small in the low-temperature phase. Given our experience with $SU(N)$, for $G(2)$ we add terms that generate the complete repulsion of eigenvalues in the low-temperature phase. Thus, the expectation value of Polyakov loops is small not because of a center symmetry but because of eigenvalue repulsion. This is also reflected in their thermodynamic behavior. With the simplest choice of parameters in our model, we find that the sharp maximum in $(e - 3p)/T^4$, found for $SU(N)$, does not appear for a $G(2)$ gauge group.

Especially given the wealth of experimental results from heavy ion collisions at ultrarelativistic energies, of course we wish to generalize this model to theories with dynamical quarks and, in particular, to QCD. Before doing so, however, we feel it is necessary to understand the transition in the pure glue theory with some care.

The outline of the paper is as follows. In Sec. II we give an introduction to how our matrix model works for the simplest case of two and three colors. We discuss the basic justification for our approach, which is a type of large-N expansion. We also discuss the quantities which the model can compute. Besides familiar quantities, such as the pressure and the Polyakov loop, this includes the 't Hooft loop, also known as the order-order interface tension. We also compute the order-disorder interface tension at T_c in our model.

There are, of course, other effective models that treat the theory near T_c. Besides the quasiparticle models discussed above [25,27], these include $Z(N)$ effective theories [42]; solutions of the functional renormalization group [43]; and Polyakov loop models [44,45]. Recent work on matrix models includes Refs. [28,34,46–48].

We stress that we are *not* attempting to solve the theory near the deconfining transition but only to develop an effective theory. As such, we find it notable that our model, with only two parameters, provides a good fit to two *functions* of temperature: both to the pressure and to the 't Hooft loop. While our two parameters are N dependent, allowing this provides a good fit to $SU(N)$ for all N.

Analyses that study the deconfining phase transition from the fundamental theory include monopoles [49], dyons [50–52], and bions [53–55]. Dyons predict that the deconfining transition is of first order for $N > 3$ and for $G(2)$, as we find [51]; they do not make detailed predictions for the thermodynamic behavior near T_c, though. Bions are especially useful in expanding about the supersymmetric limit.

In Sec. III we discuss the types of matrix model that can be constructed for arbitrary classical groups. We emphasize the role that invariance play under the Weyl group and the utility of understanding the concept of the Weyl chamber.

In Sec. IV we discuss models relevant to $SU(N)$, up to those with two free parameters. We introduce a technical assumption, which we call the ansatz of uniform eigenvalues, which allows us to compute many quantities analytically for arbitrary N. We also compare to lattice results on the interaction measure and, especially, the latent heat.

In Sec. V we compute some of the interface tensions that arise. The order-disorder interface for arbitrary N is computed analytically under the uniform eigenvalue ansatz. For two colors, we evaluate the 't Hooft loop analytically. For three colors, the 't Hooft loop is computed numerically.

The numerical solution of the model for four to seven colors is given in Sec. VI. We find that for the interaction measure and the Polyakov loop, the uniform eigenvalue ansatz works remarkably well for these values of N.

In Sec. VII we demonstrate that matrix models naturally explain why the deconfining transition is of first order not just for three colors [35] but for four or more. We consider matrix models for the $G(2)$ group in Sec. VII. A summary and conclusions are given in Sec. IX.

II. OUTLINE OF THE METHOD

In this section we give an elementary overview of how our matrix model works for two and three colors. Because we treat general gauge groups later, here we shall concentrate on the assumptions implicit in our approach and the physical quantities that we can compute in our model.

A. Two colors

General results and lattice simulations show that the expectation value of the Polyakov loop changes near T_c. To model this, we take the simplest ansatz which will generate such an expectation value, taking A_0 to assume a constant, nonzero value. By a gauge rotation we can take the background field for A_0. to be diagonal. For two colors there is only one diagonal direction, along the Pauli matrix σ_3,

$$A_0 = \frac{\pi T}{g} q\sigma_3, \qquad \sigma_3 = \begin{pmatrix} 1 & 0 \\ 0 & -1 \end{pmatrix}. \tag{3}$$

In this background field the Wilson line is

$$\mathbf{L}(\vec{x}) = \mathbf{P}\exp\left(ig\int_0^{1/T} A_0(\vec{x},\tau)d\tau\right) = \begin{pmatrix} e^{i\pi q} & 0 \\ 0 & e^{-i\pi q} \end{pmatrix}, \tag{4}$$

and the Polyakov loop, in the fundamental representation, is

$$\ell = \frac{1}{2}\,\mathrm{tr}\mathbf{L} = \cos(\pi q). \tag{5}$$

The usual perturbative vacuum is $q = 0$, $\mathbf{L} = \mathbf{1}$, and $\ell = 1$. The $Z(2)$ transform of the usual vacuum is $q = 1$, $\mathbf{L} = -\mathbf{1}$, and $\ell = -1$.

In what follows it is convenient to restrict the variable q to lie in the region q: $0 \to 1$. If we do so, a $Z(2)$ transformation is given by

$$q \to 1 - q\text{: } \mathbf{L} \to (-)\begin{pmatrix} e^{-i\pi q} & 0 \\ 0 & e^{i\pi q} \end{pmatrix}; \quad \ell \to -\ell. \tag{6}$$

Notice that this Wilson line is only -1 times that in Eq. (4) after allowing for permutation of the eigenvalues.

The confining vacuum is

$$q_c = \frac{1}{2}\text{: } \mathbf{L}_c = \begin{pmatrix} i & 0 \\ 0 & -i \end{pmatrix}, \qquad \ell_c = 0. \tag{7}$$

Given the known behavior of the Polyakov loop near T_c, this ansatz must characterize, at least to some extent, the deconfining phase transition. The essential question of physics is the following. For example, in the confined phase does ℓ_c vanish because it is dominated by q_c or because fluctuations, about various values of q, wash it out?

For an infinite number of colors, at any temperature the vacuum is dominated by a *master field.* At a nonzero temperature, the matrix q represents the master field about T_c, in the region where the value of the Polyakov loop changes. As is typical of large N, fluctuations in disconnected quantities, such as the Polyakov loop, are suppressed by powers of $1/N^2$. We stress that at a given temperature T, we can only deduce what the value of q is from measurements on the lattice. These measurements also give us no insight into which effective theory determines this q.

We now make the egregious assumption that a large-N expansion is a good approximation for all values of N, even for $N = 2$. As discussed in the Introduction, Sec. I, there are many similarities between the transitions for small and large N. A standard large-N expansion would imply computing at infinite N and then expanding in $1/N^2$. Instead, we adopt a more expansive view and assume that we can expand about q's appropriate to a given value of N. This can be considered as a type of *generalized* large-N expansion. By expanding directly in the q's appropriate to a given N, we are directly incorporating some subset of corrections in $1/N^2$ more directly than if we had followed the standard approach. This is also natural, since for either large or small N, we can only construct our effective theory with the input of lattice data.

This leaves open the question of how we could systematically develop a procedure for computing corrections to our generalized large-N expansion. There will certainly be corrections in both $1/N$ and in powers of the coupling constant, g^2. We defer this analysis for now and proceed in developing an approximation to what is certainly lowest order.

The simplest thing to do is to compute the free energy in the presence of the background field in Eq. (3). This is a standard computation; see, e.g., Sec. 2 of Ref. [56]. It will be done for a general gauge group in Sec. III. The result is

$$\mathcal{V}_{\mathrm{pt}}(q) = \pi^2 T^4\left(-\frac{1}{15} + \frac{4}{3}q^2(1-q)^2\right). \tag{8}$$

For $q = 0$ this is the free energy of an ideal gas of three massless gluons. This is degenerate with $q = 1$, which reflects the $Z(2)$ symmetry of the pure glue theory.

This potential in q can be used to compute the 't Hooft loop or the order-order interface tension [56,57]. This is the action for a state which tunnels from $q = 0$ at one end of a long spatial box to $q = 1$ at the other. The computations are typical of barrier penetration in one spatial dimension and are given in Sec. V.

Perturbatively, the confined state at $q = 1/2$ is an extremal point of the potential, but a maximum. To describe the transition to a confined state, we have to add nonperturbative terms to the effective Lagrangian to force the vacuum to go from the perturbative vacua at $q = 0$ and 1 to $q = 1/2$. After a little experimentation, the nature of these terms can be guessed.

Given the behavior of the interaction measure in Fig. 1, we assume that any term is proportional to T^2. It must also be $Z(2)$ symmetric. Thus, one such term is

$$\begin{aligned}\mathcal{V}_{\mathrm{npt}} &= -\frac{4\pi^2}{3}cT^2T_c^2\left|\frac{1}{2}\,\mathrm{tr}\mathbf{L}\right|^2 \\ &= -\frac{4\pi^2}{3}cT^2T_c^2\cos(\pi q)^2.\end{aligned} \tag{9}$$

To make up the mass dimensions, we use the critical temperature, T_c. Since T_c is a manifestly nonperturbative quantity, so is this potential.

We then take the total potential as the sum of $\mathcal{V}_{\mathrm{pt}}$ and $\mathcal{V}_{\mathrm{npt}}$. At high T, where $\mathcal{V}_{\mathrm{pt}}$ dominates, the perturbative vacuum is favored. Near T_c, where $\mathcal{V}_{\mathrm{npt}}$ becomes as important as $\mathcal{V}_{\mathrm{pt}}$, the confined vacuum, $q = 1/2$, is. It is easy to check that the deconfining transition occurs for $c = -1/16$.

The problem is that the transition is not of second order but of first. That is, when $c = 1/16$, the vacua at $q = 0$ (or 1) is degenerate with the confined phase, $q = 1/2$, but there is a nonzero barrier between the two. Hence the theory stays in the perturbative QGP until T_c, when it goes directly into the confined phase with no semi-QGP in between.

This example illustrates a more general problem. For static fields, A_0 couples to the spatial degrees of freedom A_i as an adjoint scalar. Thus, when q and A_0 are nonzero, there is an adjoint Higgs phase [21,53]. Thus, in principle there could be *two* phase transitions. Besides the usual deconfining transition at T_c, there could be a second transition, at a temperature above T_c, when the theory first enters the adjoint Higgs phase. While possible, the lattice simulations give no indication of such a second transition above T_c.

To avoid this, we add terms to the effective Lagrangian to ensure that there is no chance of such a second transition developing. This is easy. If we add a term that is *linear* in q for small q, then such a term will act to generate an expectation value for q for any temperature. That is, the theory is always in an adjoint Higgs phase.

Any term that we add must respect the $Z(2)$ symmetry. Under $Z(2)$, $q \to 1 - q$. This means that we cannot add a term which is just $\sim q$, but we can add a term $\sim q(1-q)$,

$$\mathcal{V}_{\rm npt} = -\frac{4\pi^2}{15} T^2 T_c^2 c_1 q(1-q). \tag{10}$$

This model was first proposed in Ref. [20]. Meisinger and Ogilvie showed how it can arise from the expansion of a massive field in a background field $A_0 \sim q$ [20,58]. Such a term also arises in expanding about the limit of $\mathcal{N} = 1$ supersymmetry for essentially the same reason [55]. Here, we emphasize that including such a term is not optional but is essential to avoid an unwanted phase transition above T_c.

To fit to the lattice data, we find it necessary to add two more terms to the nonperturbative potential,

$$\mathcal{V}_{\rm npt} = -\frac{4\pi^2}{3} T^2 T_c^2 \left(\frac{1}{5} c_1 q(1-q) + c_2 q^2 (1-q)^2 - c_3\right). \tag{11}$$

The term $\sim c_3$ is trivial as it does not affect the expectation value of q. The term $\sim c_2$ is clearly allowed, as it is identical to the perturbative potential in Eq. (8).

We end up with a model that appears to have three free parameters. However, we need to adjust the parameters so that the transition occurs at T_c. Secondly, we need a constraint to fix the pressure in the confined phase. At large N, the pressure in the confined phase is ~ 1, relative to that $\sim N^2$ in the deconfined phase. We adopt the simplest possible convention and assume that the pressure vanishes identically at T_c^-. In practice, it would be better to fit the pressure in the confined phase to some sort of hadronic (that is, glueball) resonance gas. Because we don't do that here, we find that our model exhibits unphysical behavior for the pressure below T_c. This is entirely an artifact of our overly simplistic assumptions.

Two conditions on three parameters then leaves one free parameter. Surprisingly, we show later that fits with one free parameter do a remarkably good job of fitting the pressure and the 't Hooft loop, at least if one is not too near T_c.

The terms in $\mathcal{V}_{\rm npt}$ are clearly not unique, as we can add arbitrary powers of $q(1-q)$. Further, there is no reason why we could not add terms which are not $\sim T^2$, but T^0, *etc*. In fact, we shall have to add a fourth term, $\sim T^0 c_3'$, later, in order to fit the region near T_c for $N \geq 3$. This is then a model with two free parameters. With such a model, we can then fit the region very near T_c, including the latent heat.

Even so, we find it striking that such simple models, with at most two free parameters, can fit several functions of temperature. It satisfies one of the cardinal virtues of any good mean-field theory, which is simplicity.

(For two colors, in our theory the energy density is negative in a narrow interval, to approximately $\sim 1\%$ about T_c. This can be corrected by adding further terms to the potential. However, we do not expect our model to describe the critical region near T_c with precision).

Viewing the A_0 as an adjoint Higgs theory yields the following. When $\langle q \rangle \neq 0$, there is a splitting of masses. Since $A_0 \sim \sigma_3$, the off-diagonal components develop a mass $\sim q$, while the diagonal ones do not. All components develop an equal mass from Debye screening. In our model, with Eqs. (10) and (11), the theory is in an adjoint Higgs phase for all $T > T_c$. In practice, for the parameters of the model, this condensate is *very* small except near T_c; above $\sim 1.2 T_c$, the condensate effectively vanishes.

B. Three or more colors

For three colors the background field can lie in one of two directions,

$$\begin{aligned} A_0 &= \frac{\pi T}{3g}(q_3 \lambda_3 + q_8 \lambda_8); \\ \lambda_3 &= \mathrm{diag}(1, -1, 0); \\ \lambda_8 &= \mathrm{diag}(1, 1, -2). \end{aligned} \tag{12}$$

Except for overall constants, λ_3 and λ_8 are the usual Gell-Mann matrices.

Unlike for two colors, the two directions now have different effects. Moving along the λ_8 generates $Z(3)$ transformations: $\mathbf{L} = \mathbf{1}$ when $q = 0$ and $\mathbf{L} = \exp(2\pi i/3)\mathbf{1}$ when $q = 1$. Moving along λ_3 takes one to the confining vacuum, which is

$$\mathbf{L}_c = \mathrm{diag}(e^{2\pi i/3}, e^{-2\pi i/3}, 1); \qquad \ell_c = 0. \tag{13}$$

When $\langle q_3 \rangle \ll 1$, then the 't Hooft loop is determined simply by the path along λ_8. As discussed in Sec. V, though, near T_c, when $\langle q_3 \rangle$ is substantial, the path is along both directions.

The generalization to arbitrary Lie groups is treated in the next section. If we concentrate only upon the behavior of the pressure, then we only need consider that path to the confining vacuum, and the problem is relatively

straightforward. If we were to consider arbitrary 't Hooft loops for $SU(N)$ when $N \geq 4$, though, it would be a much harder problem.

When the transition is of first order, as is generally true for most gauge groups, then besides the order-order interface tension, there is, at T_c, also an order-disorder interface tension. This describes the barrier between the deconfined and the confined phases at T_c.

III. THE EFFECTIVE POTENTIAL FOR GENERAL GAUGE GROUPS

In this section we compute the perturbative effective potential for a $SU(N)$ gauge group and discuss the general form which is consistent with the relevant symmetries. We compute in sufficient generality that the result be generalized to other classical groups or to $G(2)$, Sec. VII.

To lowest order, one computes about a constant background field,

$$\mathbf{A}_0 = \frac{2\pi T}{g}\mathbf{q}. \tag{14}$$

The basic variables of our matrix model are the eigenvalues of the Wilson line, which are gauge invariant. To leading order in the coupling constant g^2, these are given by expanding about the background field in Eq. (14). Since in general A_0 is gauge dependent, though, it is not surprising to find that the relationship between the background A_0, and the eigenvalues of the Wilson line, is more complicated beyond leading order in $\sim g^2$ [56,57,59,60].

For $SU(N)$ the only constraint on the eigenvalues is given by unimodularity:

$$q_1 + q_2 + \cdots + q_N = 0. \tag{15}$$

The number of independent q's in Eq. (16) is r, the rank of the group; for $SU(N)$, $r = N - 1$.

For $SU(N)$, $\mathbf{q}$ is a traceless, diagonal $N \times N$ matrix. The Wilson line is

$$\mathbf{L} = \exp(2\pi i\mathbf{q}) = \begin{pmatrix} e^{2\pi i q_1} & 0 & \cdots & 0 \\ 0 & e^{2\pi i q_2} & \cdots & 0 \\ \vdots & \vdots & \ddots & \vdots \\ 0 & 0 & \cdots & e^{2\pi i q_N} \end{pmatrix}. \tag{16}$$

We wish to compute the effective potential $\mathcal{V}(\mathbf{q})$. This can be done starting from the field theory path integral, keeping the eigenvalues of the Polyakov fixed to the value $\exp(i2\pi\mathbf{q})$. This can be done in a gauge-invariant way by taking traces of powers of the Polyakov loop. We need as many of these powers as there are independent eigenvalues:

$$\exp(-V_3\mathcal{V}(\mathbf{q})/T) = \int \mathcal{D}A\Pi_{n=1}^{r}\delta(\mathrm{tr}e^{2\pi i n\mathbf{q}} - \mathrm{tr}\overline{P(A_0)^n})\exp(-S(A)). \tag{17}$$

The average over the spatial volume V_3 is denoted by a bar. This path integral is up to a normalization the probability that a given configuration $\mathbf{q}$ of phases occurs in the system. As is well known, this constrained path integral is in the large-volume limit ($V_3 \to \infty$) the traditional free energy as a function of the quantum average of the loop. In perturbation theory, this path integral has been evaluated to order g^3.

What is the general form of the effective potential $\mathcal{V}(\mathbf{q})$ which we can take? The trace of the Wilson line in an arbitrary representation $\mathcal{R}$, $\mathbf{L}_\mathcal{R}$, is gauge invariant. By the character expansion, in the sum we can take only single traces, $\mathrm{tr}\mathbf{L}_\mathcal{R}$, if arbitrary representations are included [17–19].

In practice, we find it convenient to take traces of powers of loops, as

$$\mathcal{V}(\mathbf{q}) = T^4\sum_R\sum_{n\geq 1} w_n^R(t)\mathrm{tr}_R(\mathbf{L}^n + (\mathbf{L}^\dagger)^n). \tag{18}$$

The weights $w_n^R(t)$ are taken real. As we see later, using infinite sums, as in Eq. (18), allows us to write our (matrix) mean-field theory in an especially simple manner.

At high temperature, to one loop order the potential is as in Eq. (18), where only the adjoint representation appears,

$$w_n^{\mathrm{adj}} \sim \frac{1}{n^4}. \tag{19}$$

The traces in Eq. (18) involve the identities

$$\sum_{n=1}^{\infty}\frac{1}{n^{2p}}\cos(2\pi nx) = (-)^{p-1}\frac{(2\pi)^{2p}}{2(2p)!}\tilde{B}_{2p}(x), \tag{20}$$

where $\tilde{B}_{2p}(x)$ is a Bernoulli polynomial [61].

For $p = 1$ and $p = 2$ we define

$$\begin{aligned} B_2(x) &= x(1 - |x|), \mathrm{mod}\,1, \\ B_4(x) &= x^2(1 - |x|)^2, \mathrm{mod}\,1. \end{aligned} \tag{21}$$

We make the unconventional choice of defining $B_k(x) = \tilde{B}_k(x) - \tilde{B}_k(0)$, so that our B_k's vanish at the origin, $B_2(0) = B_4(0) = 0$. Outside of the range $|x| \leq 1$, they are defined to be periodic in x, modulo one. This reflects the fact that the q_i's are periodic variables.

The quantities B_2 and B_4 are the building blocks of our matrix model. Note that after the infinite summation over loops, we have a quartic polynomial in the eigenvalues of the Wilson line, the q's. We then need to make a judicious choice for the weights w_n^{adj}.

The $SU(N)$ groups have an additional global symmetry, the center group symmetry $Z(N)$. This means that the potential is the same for $\mathbf{L}$ and for $e^{2\pi ik/N}\mathbf{L}$, $k = 1, \cdots, N-1$. This symmetry limits the representations $\mathcal{R}$ to those having N-ality zero, such as the adjoint.

There is no such requirement in the absence of a center-group symmetry, as occurs for the group $G(2)$. Thus, besides the adjoint representation, which is a **14**, we can also

include the fundamental representation, which is a **7**. This is useful in Sec. VII.

A. General computation to one loop order

Our effective potential, $\mathcal{V}_{\rm tot}(\mathbf{q})$, is constructed from two quantities: a perturbative potential, $\mathcal{V}_{\rm pt}(\mathbf{q})$, in which the only mass scale is the temperature, and a nonperturbative term, $\mathcal{V}_{\rm non}(\mathbf{q})$, which involves both a nonperturbative mass scale and the temperature.

The perturbative potential is computed to one loop order order using the steepest descent method, applied to Eq. (17):

$$\mathcal{V}_{\rm pt}(\mathbf{q}) = T\,{\rm tr}\log(-D^2(\mathbf{q}))/V_3. \tag{22}$$

The trace is over all momentum and color degrees of freedom. Spin degrees of freedom are already summed over. The gauge covariant d'Alembertian $D^2(\mathbf{q})$ is

$$D_\mu(\mathbf{q}) = \partial_\mu + 2\pi i\delta_{\mu,0}[\mathbf{q},.]. \tag{23}$$

The color algebra can be diagonalized by using the Cartan basis. This is comprised of $N-1$ diagonal matrices, the Cartan generators, $\vec{H} = H_1, \ldots\ldots, H_r$, and $N^2 - N$ off-diagonal matrices, the E_α. Their commutation relations define the root vectors $\vec{\alpha}$ in Cartan space:

$$[\vec{H}, E_\alpha] = \vec{\alpha}E_\alpha, \tag{24}$$

$$[E_\alpha, E_{-\alpha}] = \vec{\alpha}\cdot\vec{H}, \tag{25}$$

$$[E_\alpha, E_\beta] = (\vec{\alpha}+\vec{\beta})E_{\alpha+\beta}, \quad \text{if } \vec{\alpha}+\vec{\beta} \text{ is a root.} \tag{26}$$

We normalize all generators as

$${\rm tr}\,(H_iH_j) = \frac{1}{2}\delta_{ij}, \qquad {\rm tr}(E_\alpha E_\beta) = \frac{1}{2}\delta_{\alpha,-\beta}. \tag{27}$$

The roots have a length proportional to the normalization of the matrices $\vec{H}$. But the combination

$$H_\alpha = \frac{\vec{\alpha}\cdot\vec{H}}{\vec{\alpha}^2} \tag{28}$$

does not depend on normalization. The commutation relations Eq. (26) tell us that the triplet $\hat{E}_{\pm\alpha} = E_{\pm\alpha}/|\vec{\alpha}|$ and H_α form a $SU(2)$-type algebra,

$$[H_\alpha, \hat{E}_{\pm\alpha}] = \pm\hat{E}_\alpha, \qquad [\hat{E}_\alpha, \hat{E}_{-\alpha}] = H_\alpha; \tag{29}$$

H_α is like σ_3, and $E_{\pm\alpha}$ like the $\sigma_\pm$. As a diagonal matrix, the $\mathbf{q}$ can be rewritten in terms of the $\vec{H}$, $\mathbf{q} = \vec{\mathbf{q}}\cdot\vec{H}$. In contrast to the q_i, the r components of $\vec{\mathbf{q}}$ are independent quantities.

The covariant derivative (23) acquires $\mathbf{q}$ dependence by acting with the commutator term on gauge-field fluctuations proportional to E_α. For a fixed root α, the d'Alembertian $-D^2(\mathbf{q})$ becomes

$$-D^2(\mathbf{q})E_\alpha = ((2\pi T(n+\vec{\alpha}\cdot\vec{\mathbf{q}}))^2 + \vec{p}^2)E_\alpha; \tag{30}$$

the Matsubara frequency is $2\pi Tn$, where n is an integer.

Finally, integrating over the spatial momenta, and summing over the n's and the α, gives the one-loop perturbative potential

$$\mathcal{V}_{\rm pt}(\mathbf{q}) = -\frac{(N^2-1)\pi^2}{45}T^4 + \frac{2\pi^2}{3}T^4\sum_\alpha B_4(\vec{\alpha}\cdot\vec{q}), \tag{31}$$

where B_4 is given in Eq. (21).

The arguments $\vec{\alpha}\cdot\vec{q}$ can be rewritten as $\vec{\alpha}\cdot\vec{\mathbf{q}} = 2\,{\rm tr}(\vec{\alpha}\cdot\vec{H}\mathbf{q})$. Below, we write this argument explicitly for the four types of classical groups, using standard group theory [62]. We split the $\vec{\alpha}$ into $\vec{\alpha}\to\vec{\alpha}^-$, $\vec{\alpha}^+$ and $\vec{\beta}$. Definitions of these quantities, and a detailed analysis, will appear separately [58]; here, we simply present the results.

For $SU(N)$ the argument becomes

$$\vec{\alpha}^-_{ij}\cdot\vec{\mathbf{q}} = 2\,{\rm tr}\vec{\alpha}^-_{ij}\cdot\vec{H}\mathbf{q} = q_i - q_j, \quad 1\le i<j\le N. \tag{32}$$

For the orthogonal groups $SO(2N)$, these arguments involve both differences and sums of the q_i, $2N(N-1)$ in total, living in the Cartan algebra of N dimensions:

$$\begin{aligned}&\vec{\alpha}^-_{ij}\cdot\vec{\mathbf{q}} = q_i - q_j;\\ &\vec{\alpha}^+_{ij}\cdot\vec{\mathbf{q}} = q_i + q_j, \qquad 1\le i<j\le N,\end{aligned} \tag{33}$$

together with roots of the opposite sign.

For $SO(2N+1)$ groups, the dimension of the Cartan subalgebra is the same as that of $SO(2N)$. Apart from the $2N(N-1)$ roots involving $\alpha^\pm_{ij}\cdot\vec{\mathbf{q}} = q_i \pm q_j$, as in Eq. (33) there are also $2N$ short roots β_i leading to

$$\pm\,\vec{\beta}_i\cdot\vec{\mathbf{q}} = \pm q_i, \qquad 1\le i\le N. \tag{34}$$

For the symplectic groups $Sp(2N)$ [rank N and dimension equal to that of $SO(2N+1)$], the arguments are obtained simply by leaving the $2N(N-1)$ projections $\alpha^\pm_{ij}\cdot\vec{q} = q_i \pm q_j$ the same, but changing the $2N$ short roots into long roots. This gives

$$\pm\,\vec{\beta}_i\cdot\vec{\mathbf{q}} = \pm 2q_i, \qquad 1\le i\le N. \tag{35}$$

Transforming the generic root $\vec{r}$ into its dual, $\vec{r}* = r/\vec{r}^2$, leaves the $\vec{\alpha}^\pm$ invariant, while the short roots $\vec{\beta}$ transform into the long roots and vice versa. The root systems of $SU(N)$ and of $SO(2N)$ are invariant under this transformation. The root systems of $SO(2N+1)$ and of $Sp(2N)$ transform into one another, Eqs. (34) and (35). The duality between the roots of $Sp(2N)$ and $SO(2N+1)$ implies a duality between the potentials for $\mathbf{q}$; see, also, the discussion following Eq. (155) [58].

The root system of the exceptional group $G(2)$ is dealt with in Sec. VII. There, we will use the projections in Eqs. (32)–(34) for $SU(7)$ and $SO(7)$.

B. Weyl groups and Weyl chambers

An interesting aspect of Eq. (31) is that it is a sum over *all* roots of the gauge group. This guarantees that the potential is invariant under the symmetries of the roots, which comprise the Weyl group. This invariance is especially useful in generalizing our potential to other gauge groups, such as $G(2)$ in Sec. VII.

Weyl transformations are generated by the the reflection of the simple root $\vec{\alpha}$ into the mirror, M_β, which is orthogonal to the simple root $\vec{\gamma}$. This reflection produces another root $\vec{w}_\gamma(\vec{\alpha})$:

$$\vec{w}_\gamma(\vec{\alpha}) = \vec{\alpha} - 2\frac{\vec{\alpha}\cdot\vec{\gamma}}{\vec{\gamma}^2}\vec{\gamma}, \tag{36}$$

where

$$2\frac{\vec{\alpha}\cdot\vec{\gamma}}{\vec{\gamma}^2} = m, \tag{37}$$

and m is an integer. Equation (37) is invariant under the interchange of α and γ, although the integer m may change. Together these conditions imply that the the roots lie on a lattice. The only possible angles between adjacent roots are 30°, 45°, 60°, and 90°; the relative lengths between $|\vec{\alpha}|$ and $|\vec{\gamma}|$ can be 1, $\sqrt{2}$, or $\sqrt{3}$.

To use representations other than the adjoint, we need their weight vectors, $\vec{v}$. Equation (37) is invariant if $\vec{v}$ is replaced by $\vec{\alpha}$.

Classical groups have root systems with at most two different lengths:

(i) $SU(N)$ and $SO(2N)$: all roots $\vec{\alpha}^\pm$ are equal.
(ii) $SO(2N+1)$: $2N$ short roots $\vec{\beta}$ and $N(2N-1)$ long roots $\vec{\alpha}^\pm$, $\sqrt{2}$ longer.
(iii) $Sp(2N)$: like that for $SO(2N+1)$, except that the short and long roots are interchanged.
(iv) $G(2)$: six short roots and six long roots, of relative length $\sqrt{3}$; see Sec. VII.

The Weyl group is a set of orthogonal transformations and, therefore, leaves the length of the roots invariant. For any classical group, by Eq. (37) there are at most two lengths involved; for $SU(N)$ and $SO(2N)$, there is only one length.

For $SU(N)$ there are $N-1$ independent reflections. These generate a finite group, which is the Weyl group W. The Weyl group of $SU(N)$ is the permutation group of the N fundamental indices. Thus, the order of the Weyl group is $d_W = N!$.

Lastly, we introduce the concept of the Weyl chamber, $\mathcal{W}$. The Weyl chamber has as its walls the mirrors M_α, which are perpendicular to the root α; here, α runs through the r simple roots that span the Cartan algebra. No element of the Weyl group leaves the Weyl chamber invariant, as the resulting d_W Weyl chambers fill all of the Cartan space.

Let us return to Eq. (31), the perturbative potential for the $\mathbf{q}$'s. If we wish to consider more general potentials, we need to require that they are invariant under the Weyl group. This is constructed by exploiting the separate invariance of the roots $\alpha^\pm$ and the roots β. Instead of giving long and short roots the same weight, we can take the linear combination:

$$a\sum_\alpha (B_4(\vec{\alpha}^\pm\cdot\vec{\mathbf{q}}) + a_2 B_4(2\vec{\alpha}^\pm\cdot\vec{\mathbf{q}}) + \ldots) + b\sum_\beta (B_4(\vec{\beta}\cdot\vec{\mathbf{q}}) + b_2 B_4(2\vec{\beta}\cdot\vec{\mathbf{q}}) + \ldots). \tag{38}$$

Each term in this sum is invariant under the Weyl group. This is essential in using our approach in gauge theories other than $SU(N)$, like $G(2)$, in Sec. VII.

Once we know the potential Eq. (38) inside a Weyl chamber, we can determine it everywhere in the Cartan space by using Weyl transformations and the periodicity of the Bernoulli polynomials. The Weyl symmetry is a property of the Lie algebra. Additional symmetries, such as $Z(N)$ for a $SU(N)$ gauge group, arise from global properties of the gauge group.

C. The Weyl chamber of $SU(N)$

For $SU(N)$, there is an alternate basis for the $\vec{H}$'s that is useful in what follows. Consider the diagonal matrices $\mathbf{Y}_k$, where $k = 1, 2 \ldots N-1$:

$$\mathbf{Y}_k = \frac{1}{N}\,\mathrm{diag}(k, \ldots k, k-N, \ldots, k-N). \tag{39}$$

There are $N-k$ entries k, and k entries $k-N$, so $\mathbf{Y}_k$ has zero trace; we call them hypercharges. The $\mathbf{Y}_k$ are orthogonal to the simple roots $H_{i,i+1}$:

$$\mathrm{tr}\,(\mathbf{Y}_k H_{i,i+1}) = \frac{1}{2}\delta_{ik}. \tag{40}$$

They also obey

$$\mathrm{tr}\,(\mathbf{Y}_k\mathbf{Y}_l) = \frac{1}{N}(N\min(k,l) - kl) \geq 0. \tag{41}$$

Consequently, the angle between two hypercharges is also less than $\pi/2$.

The $\mathbf{Y}_k$ are useful because they serve as generators of elements of $Z(N)$:

$$\exp(2\pi i\mathbf{Y}_k) = \exp\left(\frac{2\pi i k}{N}\right)\mathbf{1}. \tag{42}$$

Further, the $\mathbf{Y}_k$ are the edges of the Weyl chamber of $SU(N)$. To see this, take the set of $N-2$ $\mathbf{Y}_k$ matrices, excluding $\mathbf{Y}_i$. Because of Eq. (40), this set forms the Weyl mirror $M_{i,i+1}$, which is orthogonal to the root $\alpha_{i,i+1}$.

Now form a polyhedron whose $N-1$ edges are given by the $\mathbf{Y}_k$. The rest of the edges are given by drawing edges between the endpoints of the hypercharges, Eq. (39). Then the $N-1$ Weyl mirrors $M_{i,i+1}$ are the

faces of this polyhedron. This polyhedron is the Weyl chamber. Note that by Eq. (42), the vertices of the Weyl chamber are the points corresponding to the $N-1$ elements of the center group $Z(N)$.

Consider the average of all of the hypercharges; we call this average the barycenter, $\mathbf{Y}_c$, of the Weyl chamber:

$$\mathbf{Y}_c \equiv \frac{1}{N}(\mathbf{Y}_1 + \mathbf{Y}_2 + \cdots \mathbf{Y}_{N-1}). \tag{43}$$

The corresponding element of the Lie group is

$$\mathbf{L}_c = \exp(2\pi i \mathbf{Y}_c) = \begin{pmatrix} e^{\pi i(N-1)/N} & 0 & \cdots & 0 \\ 0 & e^{\pi i(N-3)/N} & \cdots & 0 \\ \vdots & \vdots & \ddots & \vdots \\ 0 & 0 & \cdots & e^{-\pi i(N-1)/N} \end{pmatrix}. \tag{44}$$

The confining vacuum is precisely the barycenter $\mathbf{Y}_c$. This is clear from the $Z(N)$ symmetry: since by Eq. (42) the hypercharges generate elements of $Z(N)$, the barycenter, as the average of all of the hypercharges, is automatically $Z(N)$ invariant. This implies, and it can be checked, that the appropriate traces of $\mathbf{L}_c$ vanish:

$$\mathrm{tr}\,\mathbf{L}_c^k = 0, \qquad k = 1 \ldots N-1; \qquad \mathrm{tr}\mathbf{L}_c^N = \mathbf{1}. \tag{45}$$

From the explicit form of Eq. (44), we also see that the eigenvalues are equally distributed about the unit circle, with a spacing $2\pi/N$. That is, in the confined vacuum there is a uniform repulsion of eigenvalues.

The Weyl chamber is illustrated in Fig. 2 for three and four colors. This figure is useful later in Sec. VII in understanding why the deconfining transition is of first order for four or more colors.

For three colors the Weyl chamber is an equilateral triangle, with corners $\mathbf{O}$, $\mathbf{Y}_1$, and $\mathbf{Y}_2$. $Z(3)$ invariance of the potential divides the Weyl chamber into three equivalent triangles, with the invariant barycenter $\mathbf{Y}_c$ in common. Note that the loop $\mathbf{L}$ is real along the line $\mathbf{OY}_c$. By a global $Z(3)$ rotation, we can require that the minima lie along this line for any temperature.

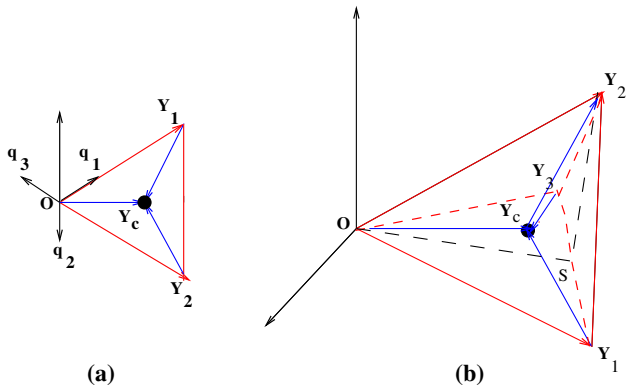

FIG. 2 (color online). The Weyl chamber for three (a) and four (b) colors. See also Fig. 12.

For four colors, the Weyl chamber is a tetrahedron, with corners $\mathbf{O}$, $\mathbf{Y}_1$, $\mathbf{Y}_2$, and $\mathbf{Y}_3$. The four faces of the tetrahedron are congruent triangles: sides $\mathbf{OY}_2$ and $\mathbf{Y}_1\mathbf{Y}_3$ have length 1, while the other four sides have length $\sqrt{3}/2$. The barycenter, $\mathbf{Y}_c$, is common to the four $Z(4)$ equivalent tetrahedrons defined by the four faces $\mathbf{OY_1Y_2}$, *etc.* We also indicate the path from the perturbative vacuum to the confining vacuum, $\mathbf{OY}_c$, and $\mathbf{OS} = \mathbf{Y}_2\mathbf{S} = 1/\sqrt{2}$. For four colors the loop $\mathrm{tr}\mathbf{L}$ is real in the plane $\mathbf{OSY}_2$, spanned by $\mathbf{OY}_{13}$ and $\mathbf{OY}_2$, and the point $\mathbf{S}$, $\mathbf{S} = (1/2)(\mathbf{Y}_1 + \mathbf{Y}_2)$.

In Fig. 2 the hypercharges $\mathbf{Y_k}$ are fixed numerical matrices. The absolute length of the roots, however, is convention dependent, and so we do not show them.

IV. ONE- AND TWO-PARAMETER MODELS FOR $SU(N)$

A. Possible potentials

To model the transition, we assume that the total potential is a sum of perturbative and nonperturbative contributions,

$$\mathcal{V}_{\mathrm{tot}}(\mathbf{q}) = \mathcal{V}_{\mathrm{pt}}(\mathbf{q}) + \mathcal{V}_{\mathrm{non}}(\mathbf{q}). \tag{46}$$

To one loop order, the perturbative potential for $\mathbf{q}$ was computed in Eq. (31), and involves

$$V_2(\mathbf{q}) = \frac{1}{2}\sum_\alpha B_4(\vec{\alpha}\cdot\vec{\mathbf{q}}), \tag{47}$$

with $B_4(x)$ given in Eq. (21). Because of the sum over the roots α, this potential is invariant under the Weyl group, and we can require the $\mathbf{q}$'s to lie in the Weyl chamber.

Given our experience with two colors in Sec. II, it is easy to guess possible forms for the nonperturbative potential. To avoid a second phase transition, above T_c, it is necessary to add a term that is linear in the $\mathbf{q}$'s for small q, as in Eq. (10). The generalization of this term for $SU(N)$ is

$$V_1(\mathbf{q}) = \frac{1}{2}\sum_\alpha B_2(\vec{\alpha}\cdot\vec{\mathbf{q}}), \tag{48}$$

where B_2 is given in Eq. (21). Summation over all roots in Eq. (48) ensures that the result is invariant under the Weyl group.

The simplest assumption is to assume that any nonperturbative term is proportional to $\sim T^2T_c^2$. Thus, we start by taking the nonperturbative potential to be

$$\mathcal{V}_{\mathrm{non}}(\mathbf{q}) = -\frac{4\pi^2}{3}T^2T_c^2 \times\left(\frac{1}{5}c_1V_1(\mathbf{q}) + c_2V_2(\mathbf{q}) - \frac{(N^2-1)}{60}c_3\right). \tag{49}$$

We shall show that with this model, we cannot explain the latent heat. Thus, we generalize the model slightly and let c_3 be temperature dependent,

$$c_3\left(\frac{T}{T_c}\right) = c_3(\infty) + (c_3(1) - c_3(\infty))\left(\frac{T_c}{T}\right)^2. \tag{50}$$

Given how $c_3(t)$ enters the potential, this is equivalent to introducing a MIT bag constant B, where

$$B = +\frac{\pi^2(N^2-1)}{45}(c_3(1) - c_3(\infty))T_c^4. \tag{51}$$

In trying to fit to the lattice data, we also tried adding terms $\sim T_c^4$ times both $B_2(\mathbf{q})$ and $B_4(\mathbf{q})$. Surprisingly, we found that the simplest possibility, Eq. (50), did the best job of fitting the lattice data.

A $SU(N)$ gauge group is invariant under charge conjugation symmetry. This is generated by $\mathbf{A}_0 \to -\mathbf{A}_0$ or $\mathbf{q} \to -\mathbf{q}$. Requiring each q_i to lie in the region between 0 and 1, this is equivalent to $\mathbf{q} \to \mathbf{1} - \mathbf{q}$. This is why the powers of $q(1-q)$ enter in the B_{2n}.

We turn to parametrizing the path between the perturbative vacuum, $\mathbf{q} = \mathbf{0}$, and the confining vacuum, $\mathbf{Y}_c$. By a global $Z(N)$ rotation, we can assume that the Wilson line $\mathbf{L} = \mathbf{1}$ at high temperature and that the trace of the Wilson line remains real for all temperatures.

For an even number of colors, we generalize the two color solution of Eq. (3): for $SU(2M)$, we take M pairs of eigenvalues, $\pm q_i$, $i = 1 \ldots M$. For an odd number of colors, $N = 2M + 1$, we take one eigenvalue to vanish, leaving again M pairs $\pm q_i$. Thus, the stationary point of the potential $SU(2M)$ or $SU(2M+1)$ involves M-indepndent variables.

The simplest possible path is a straight line from the origin to $\mathbf{Y}_c$:

$$\mathbf{q}(s) = s\mathbf{Y}_c, \qquad 0 \le s \le 1, \tag{52}$$

where

$$q_j(s) = \frac{N - 2j + 1}{2N}s. \tag{53}$$

We stress that this is an ansatz. It applies for two or three colors but is *not* a solution for four or more colors. This ansatz assumes that the M eigenvalues have constant spacing: for $2M$ colors, by reordering the eigenvalues, we have $q_j = jq_1$, $j = 1 \ldots M$, with the other M eigenvalues given by $-q_j$. In the limit of infinite N, this ansatz gives a uniform eigenvalue density to some maximum. We thus refer to Eq. (53) as the *uniform eigenvalue ansatz*.

The advantage of making the uniform eigenvalue ansatz is that it is then easy to compute *analytically* for arbitrary N. For finite $\infty > N > 3$, the exact solution must be determined numerically. We do so for four to seven colors in Sec. VI. For these values of N, we find that the difference between the uniform eigenvalue ansatz and the exact solution is remarkably small. The differences are naturally greatest at T_c. For $N = 4$ to 7, for all thermodynamic quantities and for the expectation value of the Polyakov loop, even at T_c the difference between the uniform eigenvalue ansatz and the exact solution is less than $\sim 1\%$. This difference is within the width of the curves in the figures given below. Thus, we do not present these (coincident) curves and give results only for the eigenvalues themselves in Sec. VI.

The difference between the constant eigenvalue ansatz and the exact solution increases with the number of colors. At infinite N, the model can be solved analytically [47]. At the transition, the ansatz gives an opening angle of $\frac{\pi}{4}$, Eq. (72), and a loop $\ell(T_c^+) = \frac{2}{\pi} \sim 0.64$, Eq. (74). For the exact solution the eigenvalue density is $\rho(q) = 1 + \cos(2\pi q)$ at T_c^+. This vanishes at the endpoint of $q = \frac{1}{2}$, with an opening angle of $\frac{\pi}{2}$; the loop is $\ell(T_c^+) = \frac{1}{2}$. Rescaled as in Eq. (91), the latent heat is ~ 0.16 with the ansatz, Eq. (93), and $\frac{1}{\pi^2} \sim 0.10$ from the exact solution. Thus, the latent heat is even smaller with the exact solution; this necessitates using the two-parameter model developed below.

In particular, the exact solution for large N exhibits a Gross-Witten-Wadia transition, with critical first-order behavior at T_c [47]. There is no sign of this with the uniform eigenvalue ansatz. However, to see the putative critical behavior of the specific heat, one must probe very large values of N, $N \ge 40$, and look very close to the transition, with $\sim 0.2\%$ of T_c.

Thus, given that it can be solved so easily analytically, it is instructive to study the uniform eigenvalue ansatz in some detail. We now do so for the remainder of the section.

B. Evaluating the potential under the uniform eigenvalue ansatz

From Eq. (32),

$$\vec{\alpha}_{ij}^- \cdot \vec{\mathbf{q}} = q_i - q_j = \frac{i-j}{N}s. \tag{54}$$

The perturbative vacuum is given by $s = 0$, $\mathbf{L} = \mathbf{1}$, while the confined vacuum is $s = 1$, where $\mathbf{L} = \mathbf{L}_c$, Eq. (44). The variable s is also convenient because the effective potential is $\sim N^2$, times a potential of s. The coefficients of this potential have a smooth limit at $N \to \infty$.

We need to compute

$$V_k(\mathbf{q}) = \sum_{1 \le i < j \le N} B_{2k}(q_i - q_j). \tag{55}$$

These potentials involve the sums

$$\mathcal{S}_n = \sum_{j=1}^{N}\sum_{k=1}^{N}|j-k|^n = 2\sum_{j=1}^{N}\sum_{k=1}^{j-1}(j-k)^n = 2\sum_{j=1}^{N}\sum_{k=1}^{j-1}k^n. \tag{56}$$

The last identity follows by relabeling $j - k \to k$.

We need the first four sums,

$$\mathcal{S}_1 = \frac{1}{3}N(N^2-1); \qquad \mathcal{S}_2 = \frac{1}{6}N^2(N^2-1);$$
$$\mathcal{S}_3 = \frac{1}{30}N(N^2-1)(3N^2-2); \tag{57}$$
$$\mathcal{S}_4 = \frac{1}{30}N^2(N^2-1)(2N^2-3).$$

Since the only mass scale in our model is set by the critical temperature T_c, we introduce the dimensionless ratio

$$t = \frac{T}{T_c}. \tag{58}$$

It is convenient to redefine the potential as

$$\mathcal{V}_{\rm tot}(s,t) = \frac{\pi^2(N^2-1)}{45}T_c^4 t^2(t^2-c_2)\mathcal{W}(s,t), \tag{59}$$

where

$$\mathcal{W}(s,t) = \frac{1}{t^2-c_2}\left(-t^2 - 2c_1\left(s-\frac{s^2}{2}\right) + c_3(t)\right) + 5s^2 - 6\left(1-\frac{2}{3N^2}\right)s^3 + 2\left(1-\frac{3}{2N^2}\right)s^4. \tag{60}$$

The first term, $-t^2/(t^2-c_2)$, is the ideal gas term. That $\sim c_1$ is from $B_2(\mathbf{q})$ in the nonperturbative potential, as is the constant $\sim c_3$. The quartic potential in s arises from $B_4(\mathbf{q})$, in both perturbative and nonperturbative terms.

To simplify the expressions, we let c_3 be independent of temperature; in Sec. IV B 3 we show that it is trivial to incorporate.

Fixing the parameters is done as for two colors. We start with a model with three parameters, c_1, c_2, and c_3. To destabilize the perturbative vacuum, c_1 must be positive. As it stands, T_c is just a mass parameter. One of the parameters, say c_1, can be fixed by requiring that T_c is the temperature for the phase transition.

We also need a condition to fix the value of the pressure at T_c. We make the somewhat unphysical choice that the pressure vanishes at the transition, which implies

$$\mathcal{V}_{\rm tot}(s=1,t=1) = 0. \tag{61}$$

This is used to determine c_3.

That leaves c_2 as one free parameter. We shall solve the model for arbitrary values of c_2 and determine its value by comparison to the lattice data in the next section. The value of c_2 is tuned to ensure there is a sharp peak in the interaction measure, as seen in numerical simulations.

Given the s dependence of the potential, it is useful to introduce the parameter

$$z(t) = \frac{c_1}{t^2-c_2}. \tag{62}$$

We also introduce

$$r = 1 - s. \tag{63}$$

In this variable, $r = 0$ is the confining vacuum, and $r = 1$ is the perturbative vacuum.

The value of the potential in the confined vacuum is

$$\mathcal{W}(0,t) = \frac{1}{N^2} + \frac{(-c_1-c_2+c_3)}{t^2-c_2}. \tag{64}$$

The r-dependent terms in the potential are

$$\mathcal{W}(r,t) - \mathcal{W}(0,t) = -\left(1+\frac{6}{N^2}-z(t)\right)r^2 - 2\left(1-\frac{4}{N^2}\right)r^3 + \left(2-\frac{3}{N^2}\right)r^4. \tag{65}$$

Before proceeding to the details of the solution, we make a general remark, which we expand upon later. In Eq. (65) we have reduced our model to a standard mean-field theory, with terms which are quadratic, cubic, and quartic in r. The term linear in r vanishes because the confining vacuum is necessarily extremal in r. This follows because $\mathbf{Y}_c$ is the barycenter of the Weyl chamber.

When $N = 2$, the term cubic in r vanishes, and the model has a second-order phase transition.

For three or more colors, though, the cubic term is nonzero. By standard mean-field theory, this implies that the deconfining transition is of first order for three *or more* colors. Clearly, the coefficient of the r^3 term in Eq. (65) is special to our model. We argue in Sec. VII, though, that generally the term cubic in r is nonzero. That is, the first-order transition for $N \geq 3$ is not an accident of the particular form of our model.

The vacuum at a given temperature, $r_0(t)$, is given by requiring that it is an extremum of the potential,

$$\frac{\partial}{\partial r}\mathcal{V}_{\rm tot}(r,t)\Big|_{r=r_0(t)} = 0. \tag{66}$$

The vacuum at a temperature $T = tT_c$ is the minimum, $r_0(t)$. Note that $r_0(t)$ is temperature dependent solely because $z(t)$ is.

The pressure is minus the value of the potential at this minimum,

$$p(T) = -\mathcal{V}_{\rm tot}(r_0(t),t). \tag{67}$$

The equation of motion gives a quadratic equation for r which is easily solved. The solutions are $r = 0$ and

$$r_{0\pm}(t) = \frac{1}{8(1-3/(2N^2))}\left(3\left(1-\frac{4}{N^2}\right) \pm \sqrt{25-16\left(1-\frac{3}{2N^2}\right)z(t)}\right). \tag{68}$$

As $t \to \infty$, $z(t) \to 0$, and one can see that r_{0+} corresponds to the minimum in the deconfined phase. We discuss the role which the other root, r_{0-}, plays in Sec. IV B 4.

1. Behavior at T_c

This gives us $r_{0+}(t)$ as a function of $z(t)$, but it does not determine the value of $z(t)$ at some temperature, such as $z(1)$.

To determine this, we first compute the value of r at the critical temperature, $r_c = r_0(1^+)$. This can be done by a trick. Remember that we require that the pressure vanishes in the confined phase, Eq. (61). Consequently, whether the transition is of first or second order, at T_c the pressure of the deconfined phase must then equal that in the confined phase and so vanish. This gives two conditions:

$$\mathcal{W}(0,1) = 0; \qquad \mathcal{W}(r_c,1) = 0. \tag{69}$$

By manipulating these two conditions, the terms involving $z(1)$ can be eliminated. Doing so immediately gives the value of r_c,

$$r_c = \frac{N^2-4}{2N^2-3}. \tag{70}$$

At the critical temperature, the potential has a simple form,

$$\mathcal{W}(r,1) = \left(2 - \frac{3}{N^2}\right) r^2 (r - r_c)^2. \tag{71}$$

This is the standard potential expected in mean-field theory. For two colors, $r_c = 0$, and at T_c there is a purely quartic potential, $\sim r^4$. For three or more colors, $r_c \neq 0$, and the potential has two degenerate minima, at $r = 0$ and $r = r_c$, as is typical of a first-order transition.

The value of r_c increases with N,

$$\begin{aligned} r_c(3) &= \frac{1}{3}; \qquad & r_c(4) &= \frac{12}{29}; \\ r_c(6) &= \frac{32}{69}; \qquad & r_c(\infty) &= \frac{1}{2}. \end{aligned} \tag{72}$$

The value of the Polyakov loop at T_c^+ equals

$$\ell_c = \frac{1}{N}\frac{\sin(N\delta)}{\sin(\delta)}; \qquad \delta = \frac{(N^2+1)\pi}{N(2N^2-3)}. \tag{73}$$

Explicitly,

$$\begin{aligned} \ell_c(3) &= .449\ldots; \qquad & \ell_c(4) &= .542\ldots; \\ \ell_c(6) &= .597\ldots; \qquad & \ell_c(\infty) &= \frac{2}{\pi} = .637\ldots. \end{aligned} \tag{74}$$

Since the Polyakov loop vanishes at T_c^-, these values are the discontinuity in the loop at T_c.

The value of r_c and ℓ_c for an infinite number of colors has a simple interpretation in terms of the eigenvalue density, which is a function of an angle $\theta = 2\pi j/N$. At infinite N, θ is a continuous variable, from $-\pi$ to π. In the perturbative vacuum, the eigenvalue density is a delta function at $\theta = 0$. In the confining vacuum, the eigenvalue density is constant, over the entire circle, from $-\pi$ to $+\pi$. Under the uniform eigenvalue ansatz, at T_c^+, the eigenvalue density is nonzero only over half the unit circle, from $-\pi/2$ to $+\pi/2$. The eigenvalue density for the exact solution at infinite N is not constant [47].

The value of $z_c = z(1)$ is found to be

$$z_c = \frac{(N^2+1)(3N^2-2)}{N^2(2N^2-3)}. \tag{75}$$

As a function of the number of colors,

$$\begin{aligned} z_c(2) &= \frac{5}{2}; \qquad & z_c(3) &= \frac{50}{27}; \qquad & z_c(4) &= \frac{391}{232}; \\ z_c(6) &= \frac{1,961}{1,242}; \qquad & z_c(\infty) &= \frac{3}{2}. \end{aligned} \tag{76}$$

Note that both r_c, Eq. (70), and z_c, Eq. (75), are independent of the parameter c_2. It can be shown that this is not special to the uniform eigenvalue ansatz but is also a property of the exact solution of our model for any N.

Given the definition of $z(t)$, Eq. (62), this determines c_1,

$$c_1 = z_c(1 - c_2). \tag{77}$$

Lastly, we can use the condition $\mathcal{W}(0,1) = 0$ to determine c_3,

$$c_3 = 1 + \left(z_c - 1 - \frac{1}{N^2}\right)(1 - c_2). \tag{78}$$

Using this value,

$$\mathcal{W}(0,t) = \frac{1}{N^2}\left(\frac{t^2-1}{t^2-c_2}\right). \tag{79}$$

The behavior of the pressure in the confined phase is deserving of comment. From Eq. (59) the pressure of the confined phase, where $s = 1$ and $r = 0$, is

$$p(T) = -\mathcal{V}_{\rm tot}(1,t) = -\frac{\pi^2}{45}\left(1 - \frac{1}{N^2}\right)(T^4 - T_c^2 T^2). \tag{80}$$

At large N, the pressure in the deconfined phase is $\sim N^2$, while that in the confined phase is ~ 1. This is satisfied by Eq. (80), but as discussed following Eq. (11), below T_c we should match to a hadronic resonance gas. This is a gas of massive glueballs and so will be a series of Boltzmann factors. If there are many massive glueballs, such as from a Hagedorn spectrum, the temperature dependence can be more involved, involving powers of $T_H - T$, where T_H is the Hagedorn temperature.

This is not what Eq. (80) represents, though. Rather, it reflects the limitations of an incomplete large-N approximation, where such a matching to a hadronic resonance gas has not been done. Equation (80) includes a *negative* pressure from two massless degrees of freedom, $-T^4$, and a positive term $\sim + T^2 T_c^2$. In the confined phase, these contributions are manifestly unphysical; for example, while the pressure is positive below T_c, the entropy is negative.

This shows that our model is applicable only in the deconfined phase, for $T \geq T_c$. Since it is explicitly motivated by an expansion in large N, using it in the confined phase, which involves corrections $\sim 1/N^2$, is dubious.

2. Latent heat

In this subsection we derive the interaction measure and so the latent heat. The interaction measure is related to the energy density, $e(T)$, and the pressure, $p(T)$, as

$$\Delta(T) = \frac{e - 3p}{T^4} = T\frac{\partial}{\partial T}\left(\frac{p}{T^4}\right) = -T\frac{\partial}{\partial T}\frac{\mathcal{V}_{\rm tot}(r_0(t), t)}{T^4}. \tag{81}$$

The temperature derivative acts both upon explicit and implicit temperature dependence. The explicit T dependence is from the overall factor of T^4 in the perturbative potential and T^2 in the nonperturbative potential. Clearly, only the latter contributes. There is also the implicit dependence of the solution, r_0, with temperature. Since r_0 is a solution of the equation of motion, Eq. (66), this contribution vanishes. Thus, the interaction measure depends only upon the nonperturbative potential at the minimum,

$$\Delta(T) = 2\frac{\mathcal{V}_{\rm non}(r_0(t), t)}{T^2} = -2\left(\frac{p(T) + \mathcal{V}_{\rm pt}(r_0(t), t)}{T^4}\right). \tag{82}$$

The latent heat is the jump in the energy density at T_c. By construction, we assume that both the pressure and the energy density vanish in the confined phase. The latent heat is then -2 times the perturbative potential at T_c. This equals

$$\frac{e(T_c)}{T_c^4} = \frac{\pi^2}{15}(N^2 - 1)f(N), \tag{83}$$

where

$$f(N) = z_c r_c^2 - \frac{1}{N^2} = \frac{(3N^8 - 31N^6 + 74N^4 - 22N^2 - 5)}{N^2(2N^2 - 3)^3}. \tag{84}$$

As for other quantities at T_c, in our model the latent heat is independent of the parameter c_2.

Note that while there is an overall factor of $N^2 - 1$ in the latent heat, the function $f(N)$ increases markedly as N does. Its value is $5/54 \sim .09$ for three colors and $3/8 \sim .375$ for an infinite number of colors. We comment upon this later when we compare to the lattice data in Sec. IV C 2.

3. Nonzero "bag" constant

The effective potential can be generalized to include terms other than those $\sim T^2$. The simplest is to include terms $\sim T^0$, as in Eq. (50). In the previous section, we found it convenient to consider c_2 as the single free parameter, with c_1 determined by Eq. (77) and c_3 by Eq. (78). Note that both are determined by the behavior of the potential at the critical temperature, $t = 1$.

Since the term proportional to c_3 is independent of r, we can generalize the previous solution immediately. Again, c_1 is fixed by Eq. (77). The quantity $c_3(1)$ is fixed by Eq. (78). This leaves $c_3(\infty)$ as a free parameter, which along with c_2, gives a model with two free parameters.

When $c_3(1) \neq c_3(\infty)$, there is an additional contribution to the interaction measure,

$$4\frac{B}{T^4} = \frac{4\pi^2(N^2 - 1)}{45}(c_3(1) - c_3(\infty))\left(\frac{T_c}{T}\right)^4. \tag{85}$$

We comment that in order to fit the thermodynamics of $SU(N)$, we need $c_3(1) > c_3(\infty)$. By Eq. (51), this corresponds to a positive sign for the MIT bag model, $B > 0$. This is physical, as the confining vacuum has negative pressure. Given the other terms in our model $\sim T^2$, though, probably not too much should be made of this.

4. Over and under heating

We can also use the potential to compute the temperature for over- and underheating. This is related to the behavior of the other root, $r_{0-}(t)$, in Eq. (68).

Overheating is the following. Suppose one increases the temperature from T_c. If the theory is originally in the confined vacuum, $r = 0$, then in thermal equilibrium, it tunnels to the deconfined phase at r_c. If we raise the temperature sufficiently quickly, however, it will stay at $r = 0$ until the quadratic term in r, about $r = 0$, vanishes; at this point, it must roll down the potential to $r_0 \neq 0$. This is the temperature for overheating, t_{oh}. From Eq. (65), the mass squared for r vanishes at a temperature

$$z_{\rm oh} = z(t_{\rm oh}) = 1 + \frac{6}{N^2}. \tag{86}$$

Using the value of z_c, we can then compute the ratio of the overheating temperature to T_c,

$$t_{\rm oh}^2 = \left(\frac{T_{\rm oh}}{T_c}\right)^2 = \frac{z_c(N)}{z_{\rm oh}(N)}(1 - c_2) + c_2. \tag{87}$$

The ratio $z_c/z_{\rm oh} = 1$ for $N = 2$; $z_c/z_{\rm oh} = 10/9$ when $N = 3$, and increases monotonically with N, and $= 3/2$ at $N = \infty$.

For two colors, $T_{\rm oh} = T_c$: as a second-order phase transition it cannot overheat.

For three or more colors, $T_{\rm oh} > T_c$. Unlike other quantities in our model at T_c, however, this ratio *does* depend upon the parameter c_2. When c_2 vanishes, $(T_{\rm oh}/T_c)^2 = z_{\rm oh}/z_c$. For three colors, for example, $T_{\rm oh}/T_c = \sqrt{10/9}$. As we make $c_2 \to 1$ (remember it must be less than one), we find that $T_{\rm oh} \to T_c$, independent of N.

That is, when c_2 is near one, the width of the transition region is narrower than for $c_2 = 0$. We shall see in the next section that the behavior of the interaction measure is even steeper than the behavior of $T_{\rm oh}/T_c$ indicates.

Nevertheless, it gives us some intuition as to why we find it necessary to choose a value of c_2 near one, at least for small N.

At very high temperature, one can check that the other root of Eq. (68), r_{0-}, is negative. As the temperature decreases, $r_{0-}(t)$ moves toward the origin. At the temperature for overheating, this root coincides with the origin, $r_{0-}(t_{\rm oh}) = 0$. This is why the mass squared for r vanishes at $r = 0$ at $t_{\rm oh}$.

As the temperature decreases below $t_{\rm oh}$, $r_{0-}(t)$ represents a maximum in the potential, between $r = 0$ and r_{0+}. This is true at the critical temperature, where by Eq. (71), $r_{0-}(1) = r_c/2$.

As the temperature is lowered below T_c, the point for $r_{0+}(t)$ represents a relative minimum, which is unstable to tunneling to the absolute minimum at $r = 0$. At the temperature for undercooling, the two minima coincide, $r_{0+}(t_{\rm uh}) = r_{0-}(t_{\rm uh})$. This gives

$$z_{\rm uc} = \frac{25N^2}{8(2N^2-3)} \tag{88}$$

or

$$t_{\rm uh}^2 = \left(\frac{T_{\rm uc}}{T_c}\right)^2 = \frac{z_c(N)}{z_{\rm uc}(N)}(1-c_2) + c_2. \tag{89}$$

At the temperature for underheating, there is no barrier for the theory at r_0 to roll down to the absolute minimum at $r = 0$. The qualitative behavior is the same as for overheating, except that the variation with N is much weaker.

C. Comparison between lattice data and the uniform eigenvalue ansatz

1. One-parameter model

In this section we review the results for the zero-parameter model of Meisinger *et al.* [20] and the one-parameter model which we analyzed before [14]. This is done for completeness and to make clear why it is necessary to generalize the model further.

We remark that in this paper the constants c_i differ from those in Ref. [14]. If we denote $\tilde{c}_i$ by those in Ref. [14], then they are related to those in the present work by

$$\begin{aligned}\tilde{c}_1 &= -\frac{2\pi^2}{15}c_1;\\ \tilde{c}_2 &= -\frac{2\pi^2}{3}c_2;\\ \tilde{c}_3 &= \frac{\pi^2(N^2-1)}{45N^2}c_3.\end{aligned} \tag{90}$$

The change in notation was made to make the results more transparent. In particular, the point where $c_2 = 1$ is special. There are terms $\sim \mathcal{V}_2(\mathbf{q})$ both in the nonperturbative potential, $\sim -c_2 T^2 T_c^2 \mathcal{V}_2(\mathbf{q})$, Eq. (49), and in the perturbative potential, $\sim T^4 \mathcal{V}_2(\mathbf{q})$, Eq. (31). When $c_2 = 1$, these terms cancel identically at T_c. Because of the lattice data, at least for small N we are driven to a point close to $c_2 = 1$.

In Fig. 3 we show the results for the interaction measure, $\Delta(T) = (e-3p)/(8T^4)$, for the zero-parameter model, $c_2 = 0$, and our optimal fit for the one-parameter model, $c_2 = 0.8297$. Note that here and henceforth, we rescale the interaction measure by the number of perturbative gluons, $N^2 - 1$.

As is clear from the figure, there is sharp discrepancy between the model with $c_2 = 0$ and $c_2 = 0.8297$. With the zero-parameter model, the peak in the interaction measure is off by about $\sim$50%. By introducing c_2, we can fit this to within a few percent. To do so, we have to take a value very near one.

The difference between the models is only clear once one plots the interaction measure. If one were to plot the pressure or energy density, scaled by T^4, it would be difficult to see the difference between the two models.

We remark, however, that this behavior is similar to what is seen in an analysis of the Schwinger-Dyson equations by Braun *et al.*, Ref. [43]. The numerical values for, e.g., $\langle r \rangle$ do not agree, but in both cases, the region in which the condensate is nonzero is unexpectedly small.

2. Latent heat

Nevertheless, the one-parameter model has serious problems near the critical temperature. For three or more colors, the transition is of first order, which is parametrized by the latent heat. We introduce a dimensionless measure of the latent heat, rescaling it by both T_c^4 and the number of perturbative gluons [12]:

$$L(N) = \frac{e(T_c^+)}{(N^2-1)T_c^4}. \tag{91}$$

On the lattice, $L(N)$ has been measured for $N = 3$ by Refs. [5,12] and $N = 4$, 6, and 8 [9,12]. Datta and Gupta [12] give a simple analytic form,

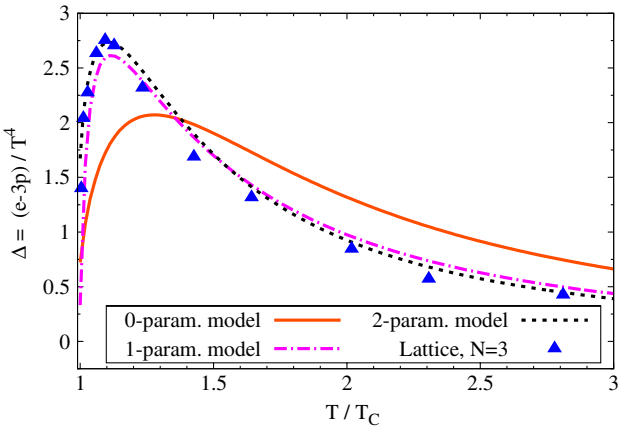

FIG. 3 (color online). A comparison of the interaction measure $(e-3p)/(8T^4)$ for three colors in the models with zero [20], one [14], and two parameters, versus lattice measurements.

$$L(N) = 0.388 - \frac{1.61}{N^2}. \tag{92}$$

We summarize these results in a Table,

N	Ref. [5]	Ref. [9]	Ref. [12]	Model
3	.175		.209	.041
4		.311	.287	.099
6		.349	.342	.137
8		.321	.363	.149
∞		.344	.388	.165

(93)

The model results are those for the one-parameter theory of the previous subsection, Eqs. (83) and (84). Remember that these values are independent of c_2.

Thus, the lattice data shows that L, while a quantity of order one, does increase from $\sim$0.2 for three colors to $\sim$0.36 for an infinite number. Our model exhibits a similar increase, but the latent heat is too small by about a factor of five for three colors and a factor of two for an infinite number. To describe the latent heat, we have to generalize the model further.

3. Two-parameter model

To ameliorate this problem, we let the parameter c_3 be temperature dependent, Eq. (50). This is equivalent to adding a MIT bag constant to the model, Eq. (51). Since only c_3 is temperature dependent, the r dependence of the potential is the same, and many results are unchanged, including the value of r_c^+, Eq. (70); the corresponding value of the Polyakov loop at T_c^+, Eq. (73); and the form of the potential in r at T_c, Eq. (71).

With two parameters, there is some freedom in how they can be chosen. For three colors, Fig. 1 shows that the rescaled conformal anomaly, $\tilde{\Delta}(T)$ in Eq. (1), is nearly constant from 1.2, to $2.0T_c$. Although the data for $N = 4$ and 6 [12] is much noisier than that for $N = 3$ [6,7], again $\tilde{\Delta}(T)$ appears to be constant over a similar range in temperature. This data also shows that the value that $\tilde{\Delta}(T)$ attains for $T > 1.2T_c$ is approximately independent of N.

From our solution, $\langle r \rangle \neq 0$ in a narrow region, below $1.2T_c$. Above this temperature, the behavior of $\tilde{\Delta}(T)$ is controlled entirely by the constant $c_3(\infty)$. Thus, we take the same value of $c_3(\infty)$ for all N. For three colors, the best value of this parameter is

$$c_3(\infty) = 0.95. \tag{94}$$

We then determined the remaining parameter, c_2, by fitting to the latent heat. To be definite, we used Eq. (92) of Ref. [12]. The results follow:

N	c_2	c_1	$c_3(1)$	$B^{1/4}$(MeV)
3	0.552	0.830	1.332	244
4	0.391	1.026	1.379	294
6	0.236	1.205	1.421	372
64	0.081	1.379	1.460	1, 249

(95)

Note that for three colors, the value of c_2 in the two-parameter model, 0.5517, is significantly smaller than for the one-parameter model, $c_2 \sim 0.8297$, Sec. IV C 1 [14]. While a relatively large change in parameters, this change is not that surprising since they were determined in rather different ways.

Fitting to the latent heat, c_2 becomes small as N increases. For infinite N, the value of c_2 is very close to zero. We have no insight as to why this is true, but it is certainly indicated by the lattice data and the form of the model.

We find that in all cases, $c_3(1) > c_3(\infty)$, so that the MIT bag constant, B, as computed from Eq. (51), is positive. The numerical value of B was determined by taking $T_c = 270$ MeV. The B constant increases with N; since $c_3(1)$ is relatively insensitive to N, this mainly reflects the definition, $B \sim N^2$ in Eq. (51).

A positive sign for the bag constant is in contrast to alternate models of the semi-QGP, such as that of Begun *et al.* [23]. In their model, the pressure is a power series in T^4, T^2, and T^0, with fixed coefficients and no dynamical fields. They find that in order to fit interaction measure, the bag constant must be negative. Their model is equivalent to ours above $\sim 1.2T_c$, where $\langle r \rangle \approx 0$, but not closer to T_c, where $\langle r \rangle \neq 0$. Indeed, having fixed $c_3(\infty)$, by Eq. (51) the bag constant follows from $c_3(1)$. Fitting to the latent heat gives $c_3(1) > c_2(\infty)$ and, thus, $B > 0$. We do not have a general argument as to why the lattice data requires $c_3(1) > c_3(\infty)$ and, so, $B > 0$.

The value of the bag constant appears sensible, although this is for the pure glue theory. We stress again, however, that since we have terms $\sim T^2$ in the potential, not too much should be made of the value of the coefficient $\sim T^0$ or the sign of the bag constant, B. See, in particular, our comments at the end of Sec. IV B 1.

We show the results for thermodynamic quantities in the following figures: Fig. 4 for three colors, Fig. 5 for four colors, and Fig. 6 for six colors. Remember that for four and six colors, we assume that the uniform eigenvalue ansatz is valid. However, a detailed comparison to the exact solution in Sec. VI shows that the difference between the uniform eigenvalue ansatz and the exact solution is small, less than $\sim$1%.

In each figure, we show the pressure, p/T^4, one third the energy density, $e/(3T^4)$, and one third the interaction measure rescaled by T^2/T_c^2, $\tilde{\Delta}(T)$ in Eq. (1). All quantities are also scaled by the number of perturbative gluons, $N^2 - 1$.

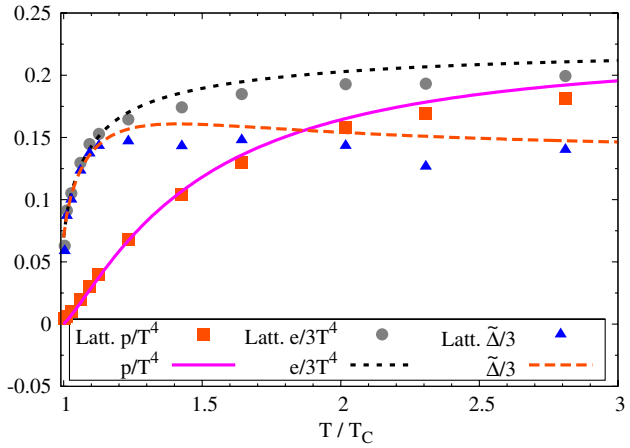

FIG. 4 (color online). Thermodynamics of SU(3): pressure p/T^4, energy density $e/(3T^4)$, and the interaction measure times T^2/T_c^2, $\tilde{\Delta}$ in Eq. (1). All quantities are also scaled by $1/8$.

Figure 7 shows the interaction measure of $SU(N)$ for various N. Overall, the model appears to reproduce the lattice data reasonably well, especially near the transition. The panel on the left zooms into the region near T_c, from T_c to $1.2T_c$. Because of the increase in the latent heat with N, $\tilde{\Delta}(T)$ increases slightly with N. Since we fit one parameter in our model to the latent heat, our model agrees well in this region. The panel on the right shows the region from 1.2 to $3.0T_c$, where the agreement between the model and the data is not quite as good. We discuss in the conclusions, Sec. IX, how this might be improved. We stress, however, that by multiplying the interaction measure by T^2/T_c^2, to form $\tilde{\Delta}(T)$, we are greatly magnifying the errors in any possible fit.

As discussed before, choosing c_2 to be near one makes the width of the transition region narrower. In Fig. 8 we

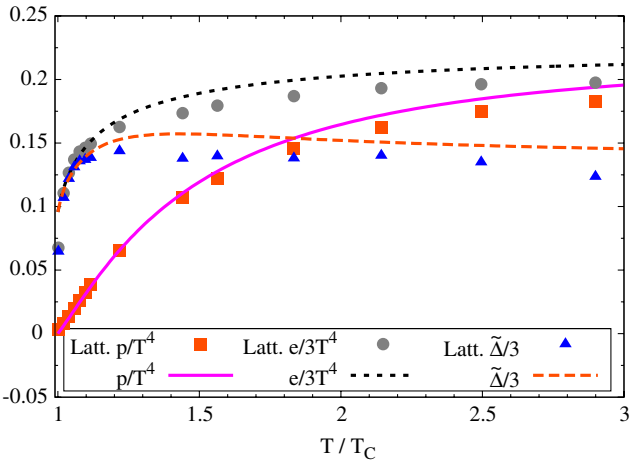

FIG. 5 (color online). Thermodynamics of SU(4) assuming the uniform eigenvalue ansatz: pressure p/T^4, energy density $e/(3T^4)$, and the interaction measure times T^2/T_c^2, $\tilde{\Delta}$ in Eq. (1). All quantities are also scaled by $1/15$.

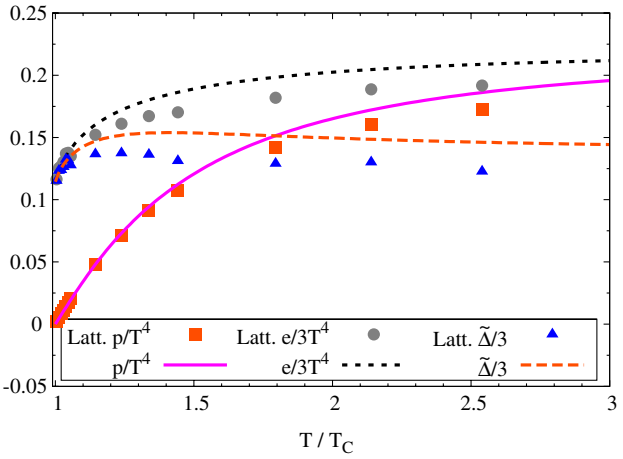

FIG. 6 (color online). Thermodynamics of SU(6) assuming the uniform eigenvalue ansatz: pressure p/T^4, energy density $e/(3T^4)$, and the interaction measure times T^2/T_c^2, $\tilde{\Delta}$ in Eq. (1). All quantities are also scaled by $1/35$.

show the result for the Polyakov loop between the models with zero, one, and two parameters. The width of the transition is broadest for zero parameters, with $c_2 = 0$, followed by that with two parameters, where $c_2 = 0.5517$, and then by that with one parameter, $c_2 = 0.8297$.

We also plot the results for the renormalized loop from lattice simulations. The results for the Polyakov loop in our model differ sharply from those obtained from the lattice. We do not understand the reason for this discrepancy and discuss this further in Sec. IX.

Lastly, in Fig. 9 we show the results for the Polyakov loop in the fundamental representation for different values of $N = 3$, 4, 6, and 64, under the uniform eigenvalue ansatz. At T_c^+, the expectation values agree with Eq. (74).

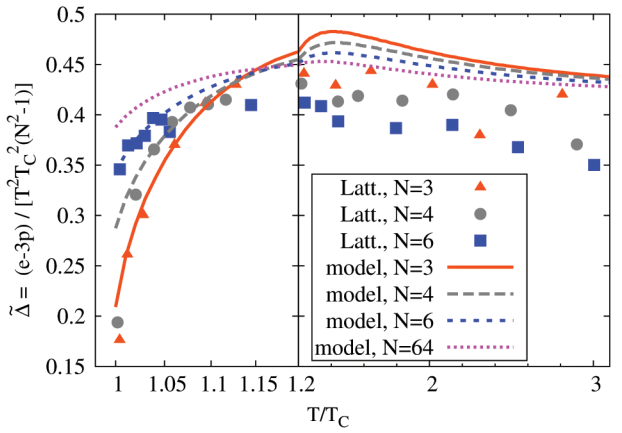

FIG. 7 (color online). Rescaled interaction measure, $\tilde{\Delta} = (e - 3p)/((N^2 - 1)T^2T_c^2)$, Eq. (1), for different values of N from our model, and the lattice. For $N = 4$, 6, and 64, we assume the uniform eigenvalue ansatz. We plot the regions $T_c \to 1.2T_c$ and $1.2T_c \to 3.0T_c$ on different abscissa scales; thus, all curves, and their derivatives, are smooth across $1.2T_c$.

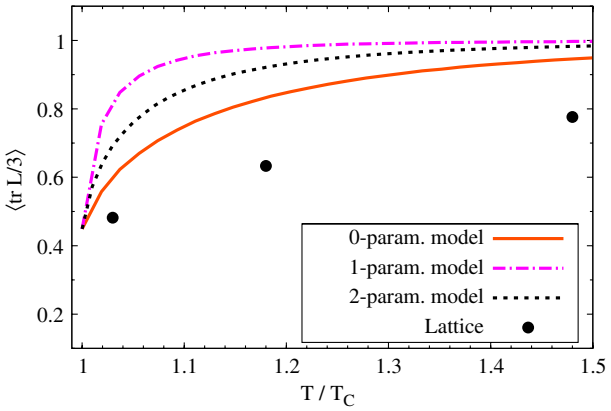

FIG. 8 (color online). A comparison of the Polyakov loop for three colors in models with zero, one, and two parameters and from lattice measurements.

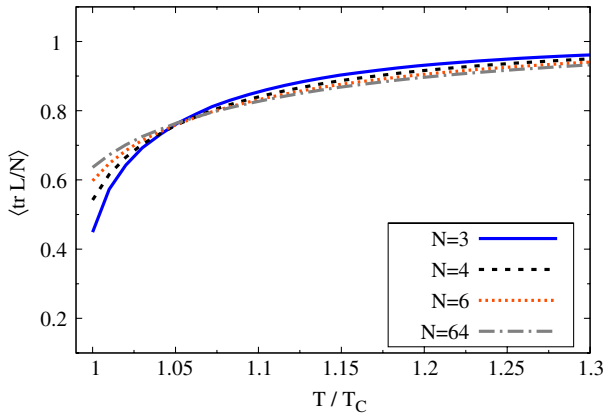

FIG. 9 (color online). Expectation values of the fundamental Polyakov loop in our model for SU(N); for $N = 4$, 6, and 64, we make the uniform eigenvalue ansatz.

They differ below $\sim 1.05T_c$, but are all rather close to one another above this temperature. This is what one expects from the conformal anomaly, which up to an overall factor of $N^2 - 1$, scales similarly for all N.

V. INTERFACE TENSIONS

An interface tension is computed as follows. Put the system in a box which is long in one spatial direction, say the z direction. Let the system be in one vacuum at one end of the box and in a degenerate but inequivalent vacuum at the other end of the box. The theory is in a vacuum state at both ends, but not in between, so forming this interface costs action. This action is proportional to the transverse volume, $V_{\rm tr}$, with the coefficient defined to be the interface tension.

Above T_c, one can have the theory in one $Z(N)$ vacua at one end of the box and a different $Z(N)$ vacua at the other. This is known as the order-order interface tension. It is equivalent to a 't Hooft loop in the deconfined phase [63]. We only compute here for two and three colors, where there is only one 't Hooft loop. For four or more colors, there is more than one 't Hooft loop, which we comment upon in the Conclusions, Sec. IX.

If the transition is of first order, as it is for $N \geq 3$, then precisely at T_c, the confined vacuum, with $r = 0$, is degenerate with the deconfined state, at $r = r_c$. This can then be used to define the order-disorder interface tension.

The computation of interface tensions in the semi-QGP is close, but not identical, to that in the perturbative QGP [56,57]. In the effective action S, in addition to the potential $\mathcal{V}_{\rm tot}(\mathbf{q})$, we need a kinetic term,

$$S = \int d\tau d^3x (\mathcal{T}_{\rm kin}(\boldsymbol{q}) + \mathcal{V}_{\rm tot}(\mathbf{q})). \tag{96}$$

In general, the kinetic term can be of the form

$$\mathcal{T}_{\rm kin}(\boldsymbol{q}) = \frac{1}{2} \sum_{a,b=1}^{N} G^{ab}(\boldsymbol{q}) \partial_i q_a(x) \partial_i q_b(x), \tag{97}$$

where $G^{ab}(\boldsymbol{q})$ is a *metric* depending on $\boldsymbol{q}$. Such a nontrivial metric arises in computing interface tensions at next-to-leading order in the coupling constant [56,57].

At leading order, however, we can use the form of the kinetic term at tree level,

$$\mathcal{T}_{\rm kin}(\boldsymbol{q}) = \frac{1}{2} {\rm tr} F_{\mu\nu}^2 = \frac{4\pi^2 T^2}{g^2} \sum_{a=1}^{N} \left(\frac{dq_a}{dz}\right)^2. \tag{98}$$

We have assumed that q_a is a function only of the long spatial direction, z, of the interface.

Assume that the vacua at the two ends of the box, $z = -L$ and $z = +L$, are Ω_i and Ω_f. These correspond to the two minima, $\bar{\boldsymbol{q}}_i$ and $\bar{\boldsymbol{q}}_f$. We take the spatial length $L \to \infty$. The interface tension is related to the shortest path between $\bar{\boldsymbol{q}}_i$ and $\bar{\boldsymbol{q}}_f$. This path obeys the equation of motion

$$\frac{8\pi^2 T^2}{g^2} \frac{d^2 q_a}{dz^2} = \frac{d\mathcal{V}_{\rm tot}}{dq_a}, \tag{99}$$

with the boundary condition $\boldsymbol{q}(-L) = \bar{\boldsymbol{q}}_i$ and $\boldsymbol{q}(L) = \bar{\boldsymbol{q}}_f$. Multiplying dq_a/dz, and integrating over z, we obtain an *energy* density,

$$\mathcal{E} = \frac{4\pi^2 T^2}{g^2} \sum_{a=1}^{N} \left(\frac{dq_a}{dz}\right)^2 - \mathcal{V}_{\rm tot}(\boldsymbol{q}). \tag{100}$$

This quantity is independent of z, so its value can be taken from either end. The kinetic term does not contribute at $z = \pm L$, so the energy is given by the potential in the vacuum, $\mathcal{E}_{\rm vac} = -\mathcal{V}_{\rm tot}(\bar{\boldsymbol{q}}_i)$.

Using the conservation of *energy*, we define

$$\delta\mathcal{V}_{\rm tot} \equiv \mathcal{V}_{\rm tot}(\boldsymbol{q}) + \mathcal{E}_{\rm vac} = \frac{4\pi^2 T^2}{g^2} \sum_{a=1}^{N} \left(\frac{dq_a}{dz}\right)^2. \tag{101}$$

The effective action becomes

$$S = V_{\rm tr}\int dz(\mathcal{T}_{\rm kin}(\boldsymbol{q}) + \mathcal{V}_{\rm tot}(\boldsymbol{q})) = S_0 + 2V_{\rm tr}\int dz\delta\mathcal{V}_{\rm tot}(\boldsymbol{q}), \quad (102)$$

where $S_0 = -2V_{\rm tr}L\mathcal{E}_{\rm vac}$. The interface tension is then

$$\alpha = \frac{1}{V_{\rm tr}}\frac{S-S_0}{T} = \frac{2}{T}\int dz\delta\mathcal{V}_{\rm tot}. \quad (103)$$

This is a general form of the interface tension. The potential depends upon the problem at hand.

A. The order-disorder interface tension under the uniform eigenvalue ansatz

The order-disorder interface is the simplest to consider. We work at the critical temperature, so we are tunneling from the deconfined state, at r_c, to the confined vacuum, at $r = 0$, and compute under the uniform eigenvalue ansatz.

From Eqs. (14) and (53), the kinetic term becomes

$$\mathrm{tr}\left(\frac{\partial A_0}{\partial z}\right)^2 = \frac{\pi^2(N^2-1)T^2}{3g^2N}\left(\frac{dr(z)}{dz}\right)^2, \quad (104)$$

where we now allow r to be a function of the spatial direction z.

At the critical temperature, the potential is

$$\mathcal{V}_{\rm tot}(r,1) = \frac{\pi^2(N^2-1)T_c^4}{45}(1-c_2)\mathcal{W}(r,1), \quad (105)$$

where the potential $\mathcal{W}(r,1)$ is given by Eq. (71). We now rescale the coordinate z as

$$\tilde{z} = \sqrt{\frac{(1-c_2)g^2N}{15}}T_c z, \quad (106)$$

so the action becomes

$$S = V_{\rm tr}\frac{T_c^3}{\sqrt{g^2N}}\frac{\pi^2(N^2-1)}{3\sqrt{15}}\sqrt{1-c_2}\int d\tilde{z}\left(\left(\frac{dr}{d\tilde{z}}\right)^2 + \mathcal{W}(r,1)\right). \quad (107)$$

Using the conservation of *energy*, the integral becomes

$$2\int d\tilde{z}\mathcal{W}(r,1) = 2\int_0^{r_c} dr\sqrt{\mathcal{W}(r,1)} = \frac{\sqrt{2N^2-3}}{3N}r_c^3, \quad (108)$$

where r_c is given in Eq. (70). Using this value, the order-disorder interface tension is given by

$$\alpha_{o-d} = \frac{T_c^2}{\sqrt{g^2N}}\frac{\pi^2}{3^{5/2}5^{1/2}}\frac{(N^2-1)(N^2-4)^3}{N(2N^2-3)^{5/2}}\sqrt{1-c_2}. \quad (109)$$

As for the order-order interface tension, this is proportional not to $\sim 1/g^2$ but to $\sim 1/\sqrt{g^2}$, because the potential for r is generated at one loop order. It is proportional to N^2 at large N, which is typical of the free energy in the deconfined phase.

To compare to the lattice, we need to assume a value for the coupling. We take $\alpha_s(T_c) = 0.3$, simply to get an idea of the numbers and, in particular, of the N dependence.

On the lattice, there are results for three colors by Beinlich *et al.* [5] and by Lucini *et al.* [9]. For four or more colors, there are results from Ref. [9].

We summarize the results for the order-disorder interface tension, α_{o-d}/T_c^2, in the following Table:

N	Ref [5]	Ref [9]	1-parameter model	2-parameter model
3	.0155	.0194	.014	.022
4		.121	.049	.093
6		.394	.167	.35
∞		$.0138N^2$	$.006N^2$	$.0139N^2$

(110)

Taken at face value, the values of the order-disorder interface tension computed in the two- parameter model agree remarkably well with those from the lattice.

This agreement could well be fortuitous. We have only included the result to leading order in the coupling constant, g^2. For the order-disorder interface tension, it is known that including at least corrections to $\sim g^2$ [56] and to $\sim g^3$ [57] are essential to obtain agreement with lattice results, even at temperatures $\sim 10T_c$, well into the perturbative QGP [64].

Even so, the fit to the latent heat indicates a lower value of c_2 in the two-parameter model than in the one-parameter model, Eq. (95). Because of the overall factor of $\sqrt{1-c_2}$ in the order-disorder interface tension, Eq. (110), the results do support a value of c_2 that decreases as N increases.

We conclude this section with a general comment. While the order-disorder interface tension is of order N^2 at large N, in fact the coefficient, from either lattice simulations or our two-parameter model, is *extremely* small, $\alpha_{o-d}/(N^2T_c^2) \approx 0.014$.

This is in sharp contrast to the latent heat, which is, properly normalized, a number of order one. For an ideal gas of N^2-1 gluons, the energy density is $(N^2-1)T^4$ times a pure number, $\pi^2/15 \sim .66$. At infinite N, by

Eq. (92) the energy density at T_c is $N^2T_c^4$ times $\sim.39$; thus, the latent heat is almost 60% the energy density of an ideal gas. This is well known from three colors: the energy density very quickly approaches that of an ideal gas, close to T_c.

Our model provides a qualitative explanation for why the latent heat is large, but the order-disorder interface tension is small. The latent heat is given by the *jump* in the order parameter, essentially by r_c. For any $N \geq 3$, this is not a small number; at infinite N, $r_c = \frac{1}{2}$, Eq. (72). Note that since r is a number between 0 and 1, we can speak of its magnitude without qualification.

In contrast, the order-disorder interface tension is given by the probability for tunneling through the barrier at T_c. Even if the jump in r is large, the probability not to tunnel through the barrier can be small if the height of the barrier is very small. That is, it is a *shallow* potential.

Such a shallow potential is exhibited by our model. For simplicity, consider the potential at infinite N. At the critical temperature, by Eq. (71) the potential is

$$\mathcal{W}(r,1)_{N=\infty} = 2r^2\left(r-\frac{1}{2}\right)^2. \tag{111}$$

The confined vacuum is at $r = 0$, while at T_c, the deconfined vacuum is at $r = 1/2$. Between $r = 0$ and $r = 1/2$, the maximum occurs at $r = 1/4$. At this maximum, the value of the potential is $\mathcal{W}(r = 1/4, 1)_{N=\infty} = 1/128$. This is certainly a barrier, but to gauge its height, consider the value of the potential at the perturbative vacuum, $r = 1$, which is $\mathcal{W}(r = 1, 1)_{N=\infty} = 1/2$. That is, the potential at the maximum of the barrier is smaller by a factor of 64 than what might have been expected. This is why the order-disorder interface tension is so much smaller than expected, because it is a broad, but very shallow, potential in r.

The above discussion holds in the uniform eigenvalue ansatz. The exact solution at infinite N is unusual and exhibits a Gross-Witten-Wadia (GWW) transition [47]. The theory appears to be a standard first-order transition, with a nonzero latent heat $\sim N^2$; see the discussion at the end of Sec. IVA. Also, for the exact solution the Polyakov loop is $\frac{1}{2}$ at T_c^+ versus $\frac{2}{\pi}$ with the uniform ansatz. Nevertheless, as $T \to T_c^+$, the loop approaches $\frac{1}{2}$ as $\sim(T - T_c)^{2/5}$, like a second-order transition. This happens because at T_c, the potential of $\mathrm{tr}\mathbf{L}$ is completely flat between the confined vacuum, at $\ell(T_c^-) = 0$, and the deconfined phase, at $\ell(T_c^+) = \frac{1}{2}$. The expectation of other loops, $\mathrm{tr}\mathbf{L}^j$ for $j \geq 2$, vanish at T_c^+.

A flat potential for the GWW transition is similar to the shallow potential found above in Eq. (111). If the potential is completely flat, then to $\sim N^2$, the order-disorder interface tension vanishes. The GWW transition is special to infinite N, so there will still be a term ~ 1.

This assumes that there is a GWW transition at infinite N. In Ref. [47] it was suggested to look for signs of the GWW transition at finite N by looking at the increase of the specific heat. This only happens at very large N, though $N \geq 40$, and only very near T_c, within $\sim 1\%$.

Perhaps another way of testing if there is a GWW transition at $N = \infty$ is to see if the order-disorder interface tension is not $\sim N^2$ but only ~ 1. Note that the value of Ref. [9] in Eq. (110) is anomalously small, $\sim.01$ times N^2. Perhaps the order-disorder interface tension might show signs of a GWW transition at values of N which are smaller than those for the specific heat.

B. The order-order interface tension for two colors

We next turn to the order-order interface tension, or 't Hooft loop, for two colors. This is simple because there is only one direction in the Weyl chamber, along the Pauli matrix σ_3. Thus moving to a confining phase, or tunneling from one $Z(2)$ vacua to another, occurs along the same direction. This greatly simplifies the computation and allows us to compute analytically, as in the previous section.

For two colors, one can show from Eq. (65) that the potential for r has a simple form,

$$\begin{aligned}\mathcal{W}(r,t) - \mathcal{W}(0,t) &= 5\left(-\frac{m(t)^2}{2}r^2 + \frac{1}{4}r^4\right);\\ m(t)^2 &= \frac{t^2-1}{t^2-c_2}.\end{aligned} \tag{112}$$

The value of the potential at $r = 0$, $\mathcal{W}(0, t)$, enters only into the vacuum energy, $\mathcal{E}_{\mathrm{vac}}$, and can be ignored.

This potential behaves as expected: the mass for r vanishes at $t = 1$, so the transition is of second order. In the deconfined phase, $t > 1$, there are two degenerate vacua, at $r(t) = \pm m(t)$. The $\pm$ represents the two degenerate $Z(2)$ vacua in the theory. At a given $t > 1$, we want to determine the tunneling probability between the $r = -m(t)$ and $r = +m(t)$.

The kinetic term is as in Eq. (104). We rescale the position as

$$\tilde{z} = \sqrt{\frac{2g^2}{3}}\sqrt{t^2-c_2}\,T_c z, \tag{113}$$

so that the action becomes

$$\frac{1}{\sqrt{g^2}}\frac{\pi^2T^2T_c}{\sqrt{6}}\sqrt{t^2-c_2}\int d\tilde{z}\left(\left(\frac{dr}{d\tilde{z}}\right)^2 + \frac{1}{5}(\mathcal{W}(r,t) - \mathcal{W}(0,t))\right). \tag{114}$$

By changing $r \to r - m(t)$, the potential, and the related integral, is precisely that of the previous section. The result for the order-order interface tension is

$$\alpha_{o-o} = \frac{4\pi^2}{3\sqrt{6g^2}}T^2\frac{(t^2-1)^{3/2}}{t(t^2-c_2)}; \tag{115}$$

remember $t = T/T_c$.

As $T \to T_c$, the order-order interface tension vanishes, as $\alpha_{o-o} \sim (T - T_c)^{3/2}$. By universality, this interface tension should vanish as $\alpha_{o-o} \sim (T - T_c)^{2\nu}$, where $2\nu \sim 1.26$; lattice results by de Forcrand *et al.* [65] find $2\nu \sim 1.32$. Our result is a type of mean-field theory, though, and so we certainly do not expect our result to correctly describe the critical region, which is very near T_c.

C. The order-order interface tension for three colors

For three colors, the path to the confined vacuum is along the $\mathbf{Y_c}$ direction, while that for the 't Hooft loop is along the $\mathbf{Y}_1$ direction in Fig. 10. Thus, we have to determine a path in two dimensions. We could not do so analytically but found a solution numerically.

We choose a vacuum in the semi-QGP as $\bar{\boldsymbol{q}}_i$,

$$\bar{\boldsymbol{q}}_i = (\bar{q}_i, 0, -\bar{q}_i), \qquad \bar{q}_i = \frac{1}{4}\left(1 - \sqrt{1 - \frac{80}{81}\left(\frac{1 - c_2}{t^2 - c_2}\right)}\right). \tag{116}$$

We wish to find a path that tunnels from this point to a $Z(3)$ transform of this point, $\bar{\boldsymbol{q}}_f$,

$$\bar{\boldsymbol{q}}_f = \left(\frac{2}{3} - \bar{q}_i, -\frac{1}{3} + \bar{q}_i, -\frac{1}{3}\right). \tag{117}$$

We parametrize this path as

$$\boldsymbol{q} = \bar{\boldsymbol{q}}_i + \left(\frac{2q_\alpha}{3}, q_\beta - \frac{q_\alpha}{3}, -q_\beta - \frac{q_\alpha}{3}\right). \tag{118}$$

The potential which governs this tunneling is

$$\delta\mathcal{V}_{\rm tot}(q_1, q_2, q_3) = \mathcal{N}_{\mathcal{V}_3}\mathcal{V}_{\rm norm}(q_\beta, q_\alpha), \tag{119}$$

where

$$\mathcal{N}_{\mathcal{V}_3} = \frac{8\pi^2}{3}T_c^4 t^2(t^2 - c_2). \tag{120}$$

Without loss of generality, we can choose the variables to satisfy $0 \le q_\alpha < 1$, $0 \le q_\beta < q_\alpha$ and $q_\beta < 1 - q_\alpha$. The potential becomes

$$\begin{aligned}\mathcal{V}_{\rm norm}(q_\beta, q_\alpha) = {} & q_\alpha^2(q_\alpha - \bar{q}_f)^2 + 2q_\alpha(q_\alpha - \bar{q}_f)(1 - \bar{q}_f)q_\beta \\ & + (6q_\alpha(q_\alpha - \bar{q}_f) + \bar{q}_f(2 + \bar{q}_f))q_\beta^2 \\ & - 2(1 + 3\bar{q}_f)q_\beta^3 + 9q_\beta^4,\end{aligned} \tag{121}$$

where $(q_\beta, q_\alpha) = (0, \bar{q}_f) \equiv (0, 1 - 3\bar{q}_i)$ corresponds to $\bar{\boldsymbol{q}}_f$.

The kinetic term is

$$\mathcal{T}_{\rm kin} = \mathcal{N}_{\rm cl3}\left[\left(\frac{dq_\alpha}{dz}\right)^2 + 3\left(\frac{dq_\beta}{dz}\right)^2\right], \tag{122}$$

where $\mathcal{N}_{\rm cl3} = 8\pi^2T^2/(3g^2)$. The interface tension becomes

$$\begin{aligned}\alpha_{o-o} &= 2\sqrt{\mathcal{N}_{\mathcal{V}_3}\mathcal{N}_{\rm cl3}}\int d\tilde{z}\,\mathcal{V}_{\rm norm}(q_\alpha, q_\beta) \\ &= \frac{16}{3g}\pi^2T^2\sqrt{1 - \tilde{c}_2 t^{-2}}\int d\tilde{z}\,\mathcal{V}_{\rm norm}(q_\alpha, q_\beta),\end{aligned} \tag{123}$$

where $\tilde{z} = gT_c\sqrt{t^2 - c_2}z$.

For two colors, the path is in one direction, and so we can use energy conservation to determine the action to tunnel, even without an explicit form of the solution. For three colors, the path is in two directions, and so energy conservation alone does not determine either the solution or its action. Thus, we need to explicitly determine the path that tunnels between the two degenerate vacua. This satisfies the equation of motion,

$$\frac{d^2q_\alpha}{d\tilde{z}^2} = \frac{1}{2}\frac{d\mathcal{V}_{\rm norm}}{dq_\alpha}, \qquad \frac{d^2q_\beta}{d\tilde{z}^2} = \frac{1}{6}\frac{d\mathcal{V}_{\rm norm}}{dq_\beta} \tag{124}$$

with the boundary conditions

$$\begin{aligned}q_\alpha(-\infty) &= 0, \qquad q_\alpha(\infty) = \bar{q}_f, \\ q_\beta(-\infty) &= 0, \qquad q_\beta(\infty) = 0.\end{aligned} \tag{125}$$

These boundary conditions do not uniquely determine the solution, because we need to specify the turning point. We require that the turning point occurs at the middle of the interface, $\tilde{z} = 0$, so that

$$q_\alpha(0) = \frac{\bar{q}_f}{2}. \tag{126}$$

This is natural, since the potential is symmetric under $q_\alpha \leftrightarrow (\bar{q}_f - q_\alpha)$. This also implies that at the turning point,

$$\frac{dq_\beta(0)}{d\tilde{z}} = 0. \tag{127}$$

At this point, the derivative of q_α is obtained by energy conservation, Eq. (101):

$$\frac{dq_\alpha(0)}{d\tilde{z}} = \sqrt{\mathcal{V}_{\rm norm}(q_\beta(0), q_\alpha(0))}. \tag{128}$$

In the numerical computations we use Eq. (128) instead of Eq. (125) as a boundary condition.

In the perturbative QGP, $\bar{q}_f = 1$ is the vacuum, so that as $t \to \infty$, the derivative $d\mathcal{V}_{\rm tot}/dq_\beta = 0$ vanishes at $q_\beta = 0$. In this case, a straight line path, along $\mathbf{Y}_1$, is a solution of the equations of motion [56].

In the semi-QGP, a straight path is not a solution to the equations of motion, and the path lies in both directions, $\mathbf{Y}_1$ and $\mathbf{Y}_2$. A solution to the equations of motion was found numerically. In Fig. 10 we show paths $(q_\alpha(z), q_\beta(z))$ in the plane of q_α and q_β. The path at T_c^+ is that which comes closest to the $SU(3)$ confining vacuum, $\mathbf{Y}_c$. Since both tr$\mathbf{L}$ and tr$\mathbf{L}^2$ vanish at $\mathbf{Y}_c$, these values are small for the point on the path closest to $\mathbf{Y}_c$, at T_c^+. That these loops are small

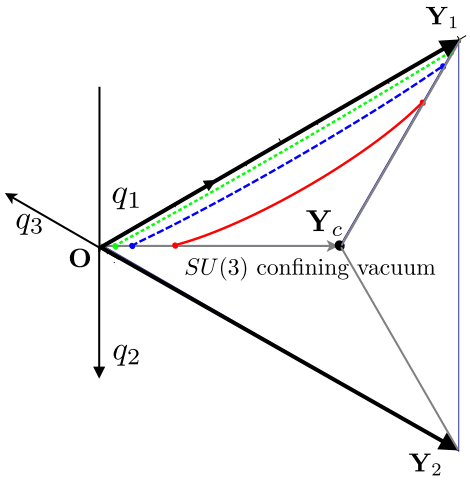

FIG. 10 (color online). Classical paths for the interface tension in a pure $SU(3)$ gauge theory. The paths curve more as the temperature decreases, as the path at T_c^+ approaches closest to the confined vacuum, $\mathbf{Y}_c$.

in the middle of the interface has been observed previously in a Polyakov loop model [45]. We also note that the interface tension has been analyzed in linear models [42].

In Fig. 11, we give the result for the order-order interface tension, α_{o-o}. We remark that while, in principle, $\langle q \rangle \neq 0$ for all temperatures, in practice this is very small except close to T_c. This means that to a good approximation, we can take a path along $\mathbf{Y}_1$ when $T > 1.2T_c$. We also note that in plotting the interface tension in our model, versus that from the lattice [66], we have included a perturbative correction $\sim g^2$. This correction was computed in the perturbative QGP and so should be recomputed for the semi-QGP. Except for $T < 1.2T_c$, however, it can be shown that this correction is correct [67].

We conclude by discussing the problem of order-order interface tensions for four or more colors. In the complete QGP, the path for order-order interface tension is along one

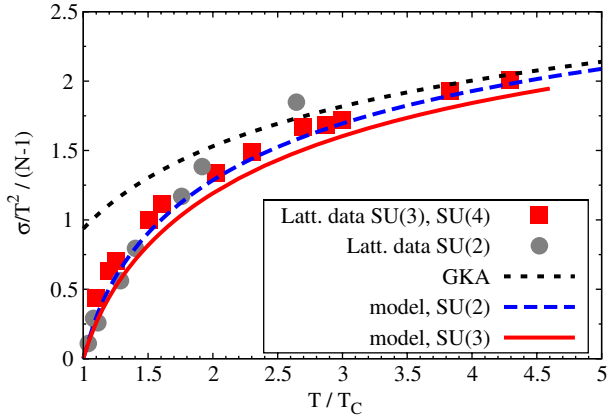

FIG. 11 (color online). The interface tension for $SU(3)$ pure gauge theory.

of the hypercharge directions, the $\mathbf{Y}_k$ of Eq. (39) [57]. The example of three colors shows, however, that near T_c the path lies in the full space of $N-1$ dimensions. This is an interesting but nontrivial exercise in minimization, which we defer for now. We comment further about these interface tensions in the Conclusions, Sec. IX.

VI. NUMERICAL SOLUTION OF THE MODEL FOR FOUR TO SEVEN COLORS

Before describing our numerical results, we first make an elementary but useful remark. As discussed preceding Eq. (52), by a global $Z(N)$ rotation we can require that the expectation value of the Polyakov loop is real. If $N = 2M$ or $2M+1$, this means that the solution involves M degrees of freedom. At infinitely high temperature all $\mathbf{q}$'s vanish. As the temperature decreases, the $\mathbf{q}$'s move along a curve in this M-dimensional space until, at the critical temperature, they end up at a point $\mathbf{q}_c^+$. At this point, the value of the potential equals that in the confined vacuum, where $\mathbf{q}_c^- = \mathbf{Y}_c$, Eq. (43). This assumes that the transition is of first order, so that $\mathbf{q}_c^+ \neq \mathbf{q}_c^-$; we justify this later in Sec. VII.

For finite $N > 3$, the path in the M-dimensional space can be determined numerically. The total potential in our model is given by

$$\mathcal{V}_{\rm tot}(\mathbf{q}) = f_0(T) + f_1(T)V_1(\mathbf{q}) + f_2(T)V_2(\mathbf{q}). \quad (129)$$

We have chosen very specific forms for the functions $f_0(T)$, $f_1(T)$, and $f_2(T)$, but the following conclusion is independent of their specific form.

The solution of the model at a given temperature, $\mathbf{q}_0(T)$, is given by requiring that the total potential is stationary with respect to the $\mathbf{q}$'s,

$$\frac{\partial \mathcal{V}_{\rm tot}(\mathbf{q})}{\partial \mathbf{q}}\bigg|_{\mathbf{q}=\mathbf{q}_0(T)} = f_1(T)\frac{\partial}{\partial \mathbf{q}}\left(V_1(\mathbf{q}) + \frac{f_2(T)}{f_1(T)}V_2(\mathbf{q})\right)_{\mathbf{q}=\mathbf{q}_0(T)} = 0, \quad (130)$$

which is the generalization of Eq. (66).

Because the $\mathbf{q}$ dependence only enters through two functions, $V_1(\mathbf{q})$ and $V_2(\mathbf{q})$, trivially this equation involves only the ratio $f_2(T)/f_1(T)$. Whatever the specific form of these two functions, at a given temperature this is a pure number.

This implies that in the M-dimensional space of the $\mathbf{q}$'s, the path is *independent* of the choice of these two functions. Further, it follows immediately that the endpoint of the path, $\mathbf{q}_c^+$, is also *independent* of this choice of these two functions.

That the endpoint is independent of these functions was observed previously for the uniform eigenvalue ansatz. We found there that at T_c the solution is independent of the one free parameter, c_2.

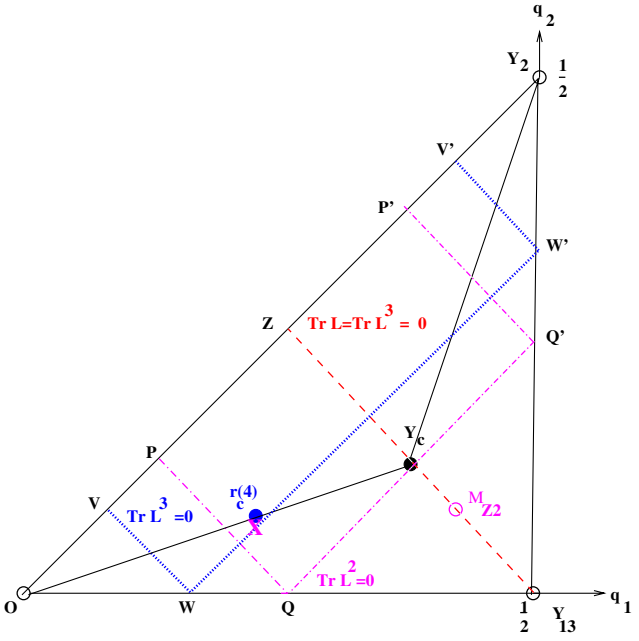

FIG. 12 (color online). For four colors, the region of the Weyl chamber where the expectation value of the Polyakov loop is real.

Needless to say, different choices of the $f_i(T)$ functions *do* give different physics. While the path in $\mathbf{q}$ space is independent of the f_i's, thermodynamic quantities also involve derivatives with respect to temperature, and these change as $f_1(T)$ and $f_2(T)$ do. That is, the temperature dependence of how one proceeds along this fixed path depends upon the choice of these functions. In the uniform eigenvalue ansatz, this is what changing the parameter c_2 does: it shifts the overall scale of T/T_c in a nonlinear fashion.

A. Four and five colors

We now turn to the case of four colors. In Fig. 12 we illustrate the region of the Weyl chamber in which the expectation value of the Polyakov loop is real. This is the plane spanned by the hypercharge $\mathbf{Y}_2$ and by $\mathbf{Y}_{13} = (\mathbf{Y}_1 + \mathbf{Y}_3)/2$.

The confining vacuum is given by the barycenter, $\mathbf{Y}_c$. The curves where $\mathrm{tr}\mathbf{L}^p$ vanish, for $p = 1, 2$, and 3, are also indicated. The uniform eigenvalue ansatz is the line $\mathbf{OY}_c$. In this ansatz, the point $\mathbf{q}_c^+$ is given by a blue point; for the exact solution, it is given by a magenta cross.

Under a $Z(2)$ transformation, the triangle $\mathbf{OY}_2\mathbf{Y}_{13}$ maps onto itself: $\mathbf{O}$ and $\mathbf{Y}_2$ interchange with one another, while the lines where $\mathrm{tr}\mathbf{L} = \mathrm{tr}\mathbf{L}^3$ vanish are left invariant.

The numerical solution for the trajectory of $SU(4)$ is plotted in Fig. 13. There are two positive eigenvalues, q_1 and q_2. In the uniform eigenvalue ansatz, $q_2 = 3q_1$. The left panel shows the path in the plane of q_1 and q_2; visually, this is obviously very close to a straight line. The right panel shows the values of q_1 and $q_2/3$; the amount by which $q_1 \neq q_2/3$ indicates the deviation from the uniform eigenvalue ansatz. Even at T_c, this deviation is very small. As discussed previously, for thermodynamic quantities, and the expectation value of the Polyakov loop, the results are within the width of the curves in Figs. 5 and 9, respectively.

In $Z(4)$ spin systems it is possible to have mixed phases between ordered and disordered phases where $Z(4)$ is broken but $Z(2)$ is unbroken. For $SU(4)$ such a $Z(2)$-invariant phase would have $\mathrm{tr}\mathbf{L} = \mathrm{tr}\mathbf{L}^3 = 0$ and $\mathrm{tr}\mathbf{L}^2 \neq 0$. For example, the point along this line where $\mathrm{tr}\mathbf{L}^2 = 1$ is indicated by the point M_{Z2}. We find no evidence for such a $Z(2)$ phase at any temperature. This agrees with numerical simulations on the lattice [68].

For five colors the plane where the Polyakov loop is real is shown in Fig. 14; it is spanned by the line $\mathbf{Y}_{14} = (\mathbf{Y}_1 + \mathbf{Y}_4)/2$ and $\mathbf{Y}_{23} = (\mathbf{Y}_2 + \mathbf{Y}_3)/2$. In this plane $\mathrm{tr}\mathbf{L}$ is real, and we expect the trajectory of the minima to again nearly coincide with the straight line *ansatz* from the origin to $\mathbf{Y}_c$, as for four colors. This is indeed the case as is evident from Fig. 15. Only near T_c do the eigenvalues of the Wilson line deviate from the straight line. Here, too, we found that the thermodynamic functions agree with those obtained above with the straight line ansatz.

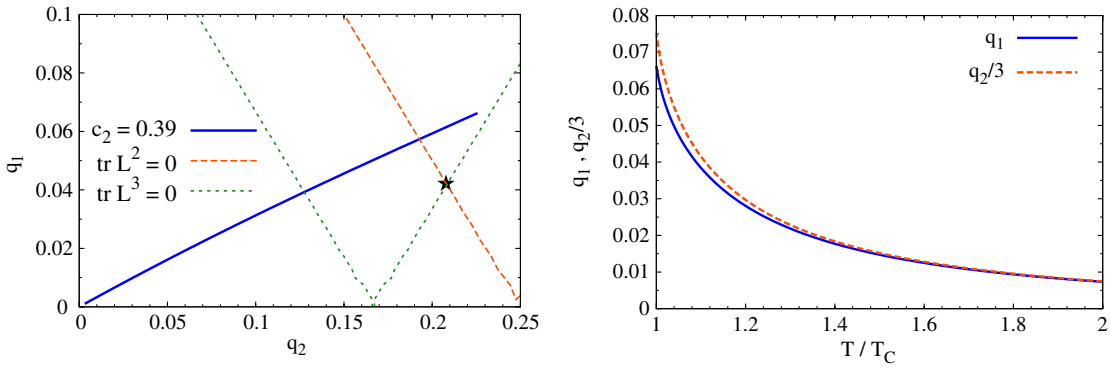

FIG. 13 (color online). The numerical solution for four colors, with $c_2 = 0.39$. The left panel is in the q_1-q_2 plane, while the right panel gives $q_2/3$ and q_1.

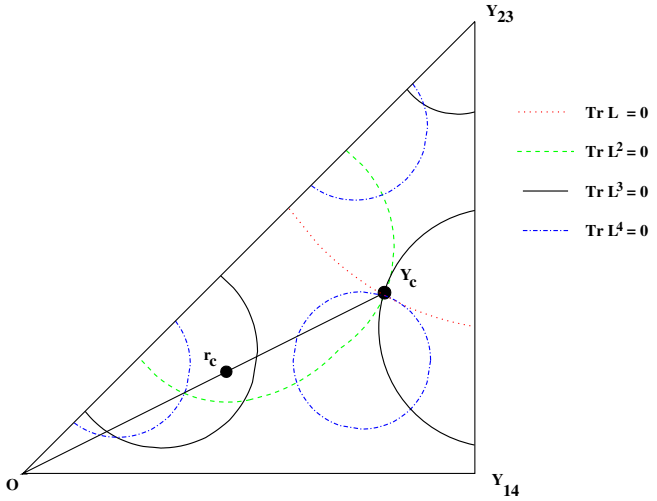

FIG. 14 (color online). For five colors, the plane where the Polyakov loop is real.

There is one feature of the uniform eigenvalue ansatz which is shared by the exact solution at infinite N [47]. This is illustrated for four colors in Figs. 12 and 13, and for five colors, by Figs. 14 and 15. For both four and five colors, $\mathrm{tr}\mathbf{L}^2$ and $\mathrm{tr}\mathbf{L}^3$ vanishes once at $T > T_c$; for five colors, $\mathrm{tr}\mathbf{L}^4$ does so twice. At infinite N, $\mathrm{tr}\mathbf{L}^2$ and $\mathrm{tr}\mathbf{L}^3$ also vanish once for $T > T_c$, and $\mathrm{tr}\mathbf{L}^4$, twice. For infinite N, the number of zeroes of $\mathrm{tr}\mathbf{L}^n$, with $n < N$, increases as n does [47].

B. Six and seven colors

In this case the space where the Polyakov loop is real is three dimensional, see Fig. 16.

For six colors we find again that the exact solution is close to that of the uniform eigenvalue ansatz. It is also possible to have intermediate phases in which there is a global $Z(2)$ or $Z(3)$ symmetry. We find no evidence of such partially deconfined phases.

We comment that the symplectic group $Sp(6)$ is the pseudoreal part of $SU(6)$; by exchanging the short and long roots of $SO(7)$, this is the dual of $Sp(6)$ [69]. As already remarked in Sec. III, to one-loop order the perturbative potentials $\mathcal{V}_{\mathrm{pert}}(\mathbf{q})$ are, therefore, related by duality. If the nonperturbative potentials are assumed to be dual as well, then the deconfining phase transitions are the same [58]. This can be tested through numerical simulations on the lattice.

In Fig. 17 we show the path for the exact solution. In the uniform eigenvalue ansatz, $q_1/2 = q_2/3 = q_3/4$. We find that the deviation from this is small except close to T_c. The results for seven colors are interesting because of their relevance for the confining states in $SO(7)$ and $G(2)$ groups, discussed in Sec. VII.

VII. WHY THE DECONFINING PHASE TRANSITION IS OF FIRST ORDER FOR FOUR OR MORE COLORS

In this section we discuss why a first-order transition is expected generically in matrix models when $N \geq 3$.

We first review the standard argument for why the transition is of first order for three colors [35]. If ℓ is the loop in the fundamental representation, we consider a general potential invariant under $Z(N)$ transformations,

$$\ell \longrightarrow \mathrm{e}^{2\pi i/N}\ell. \tag{131}$$

The corresponding potential includes two terms. First, there is

$$V_{O(2)}(\ell) = m^2|\ell|^2 + \lambda_{O(2)}(|\ell|^2)^2, \tag{132}$$

which is invariant under $O(2)$ transformations. Second, there is

$$V_{Z(N)}(\ell) = \lambda_{Z(N)}(\ell^N + (\ell^*)^N), \tag{133}$$

which is invariant only under $Z(N)$.

For three colors, Eq. (133) is a cubic invariant and is, in the sense of the renormalization group, a relevant operator. By standard mean-field analysis, the transition is of first order. We note that there is a qualification: if the coupling $\lambda_{Z(N)}$ vanishes, then the transition could be of second order

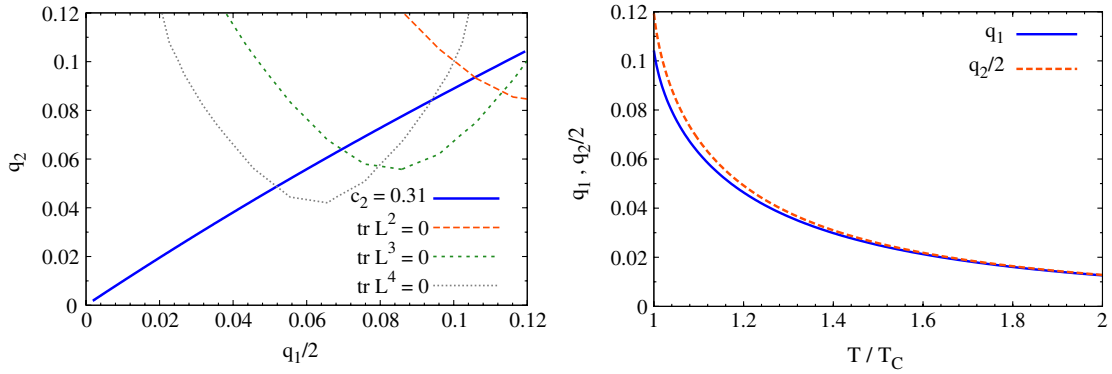

FIG. 15 (color online). The numerical solution for five colors, with $c_2 = 0.31$. The left panel is in the q_1-q_2 plane, while the right panel gives $q_2/2$ and q_1.

(if $\lambda_{O(2)} > 0$). There is no symmetry reason why $\lambda_{Z(N)}$ should vanish, though, so one expects a first-order transition.

For four colors, Eq. (133) is a quartic term and, thus, marginal. For five or more colors, it is of fifth or higher order and so an irrelevant operator. Then the deconfining transition is of second order when $\lambda_{O(2)} > 0$, and of first order when $\lambda_{O(2)} < 0$. In the latter case, a positive term $\sim(|\ell|^2)^3$ stabilizes the potential.

Why, then, is the deconfining transition of first order for any $N \geq 3$? This follows in mean-field theory from a matrix model. From Eq. (65) of Sec. III, in our particular model there is a cubic term in r about the confining vacuum, $r = 0$. As discussed there, in mean- field theory this implies that the deconfining transition is of first order.

To see that this is not an accident, consider the general form of an effective potential. We express our matrix model in terms of the q_i, and then r, but in general we can construct any function of the q_i as a series in powers of $\mathrm{tr}\mathbf{L}$, $\mathrm{tr}\mathbf{L}^2$, and so on, up to $\mathrm{tr}\mathbf{L}^{N-1}$. Each term must be invariant under $Z(N)$ transformations, so the simplest possible terms include

$$|\mathrm{tr}\mathbf{L}|^2; \quad |\mathrm{tr}\mathbf{L}^2|^2; \quad |\mathrm{tr}\mathbf{L}^3|^2; \quad (\mathrm{tr}\mathbf{L})(\mathrm{tr}\mathbf{L}^3) + \text{c.c.} + \ldots. \tag{134}$$

There is clearly an infinite series of such terms. The first three terms are invariant under $O(2)$; the last, under $Z(4)$. This multiplicity of terms is in contrast to a loop model, which only involves powers of the loop in the fundamental representation, $\mathrm{tr}\mathbf{L}$.

Now we perform an elementary computation. Take the basic ansatz for A_0, Eq. (14). We do not assume the uniform eigenvalue ansatz, Eq. (52), but consider a general path, parametrized as

$$\begin{aligned} \mathbf{q} &= (q_1, q_2, -q_2, -q_1); \\ q_1 &= \frac{1}{8}(1 - \tilde{x} + \tilde{y}); \\ q_2 &= \frac{1}{8}(3 - \tilde{x} - \tilde{y}). \end{aligned} \tag{135}$$

The confined vacuum is $\tilde{x} = \tilde{y} = 0$. For the straight line path, $\tilde{x} = 2\tilde{y}$, but this parametrization is convenient, so that the expansion in Eq. (136) has a simple form.

We can then easily compute the expansion of these quantities about the confining vacuum. We introduce $x = \pi\tilde{x}$ and $y = \pi\tilde{y}$,

$$\begin{aligned} \left|\frac{1}{4}\,\mathrm{tr}\mathbf{L}\right|^2 &= \frac{1}{2}x^2 + \frac{1}{4}x^2 y + \ldots, \\ \left|\frac{1}{4}\,\mathrm{tr}\mathbf{L}^2\right|^2 &= 4y^2 - x^2y^2 - \frac{1}{3}y^4 + \ldots, \\ \left|\frac{1}{4}\,\mathrm{tr}\mathbf{L}^3\right|^2 &= \frac{9}{2}x^2 - \frac{27}{4}x^2 y + \ldots. \end{aligned} \tag{136}$$

All of these loops vanish in the confined vacuum, $x = y = 0$; as the confined vacuum is the barycenter of the Weyl chamber, the terms linear in x and y do as well, Sec. III C. These loops then begin with terms quadratic in x and y. What is of relevance here is the existence of terms cubic in x and y, which are always $\sim x^2 y$.

The general pattern is clear. Most terms, such as $|\mathrm{tr}\mathbf{L}^2|^2$ and $|\mathrm{tr}\mathbf{L}^3|^2$, etc., have terms which are cubic in x and y. This is true for any term which involves $\mathrm{tr}\mathbf{L}^n$, for odd n. Thus, if there are *any* such terms in the effective potential, then in mean-field theory the transition is of first order. Note that having two fields doesn't alter the conclusion: the point is that one cannot obtain a *flat* potential, typical of a second-order transition. The variables x and y are useful because then the quadratic terms are diagonal.

Note that in a loop model, terms such as $|\ell|^2 \sim |\mathrm{tr}\mathbf{L}|^2$ are even in ℓ and do not give a first-order transition. A first-order transition only follows in a matrix model, where one expands about the barycenter of the Weyl chamber.

As illustrated by Eq. (136), if a term only involves $\mathrm{tr}\mathbf{L}^n$, for even n, then there is no term cubic in x and y, and the transition can be of second order. This does not invalidate the expectation of a first-order transition. If the effective Lagrangian involves only even powers of $\mathrm{tr}\mathbf{L}^n$, then the global symmetry of the theory is not $Z(4)$ but $Z(2)$. The global symmetry is then not like that expected for four colors, but like that for two colors, where the transition is of second order. However, as for the analysis of three colors in a loop model, there is no reason to expect such an accidental $Z(2)$ symmetry to occur. Indeed, for this to happen in a matrix model, an infinite number of terms would have to vanish.

The above analysis can be generalized for any $N \geq 3$. In general, there are cubic terms in the expansion of $|\mathrm{tr}\mathbf{L}^n|^2$, except for those n and N where there may be a residual $Z(n)$ symmetry in $Z(N)$, as for $n = 2$ and $N = 4$.

Why the deconfining phase transition is of first order for $N \geq 3$ can also be understood geometrically from the Weyl chamber for three and four colors in Fig. 2.

For three colors the Weyl chamber is an equilateral triangle, bounded by the vectors $\mathbf{Y}_1$ and $\mathbf{Y}_2$. The confined vacuum, $\mathbf{Y}_c$, is the barycenter of this triangle. The path from the perturbative vacuum, to the confined vacuum, is a straight line, $\mathbf{OY}_c$.

Consider expanding an effective potential about $\mathbf{Y}_c$, along this straight line. Even without computation, it is evident that the region to the right is smaller than that to the left. Thus, if we expand in r, where $r = 0$ is the confined vacuum, we would expect terms of cubic order and so a first-order transition.

For four colors, instead of considering the full three-dimensional space of the Weyl chamber, we can limit ourselves to the plane where the Polyakov loop is real,

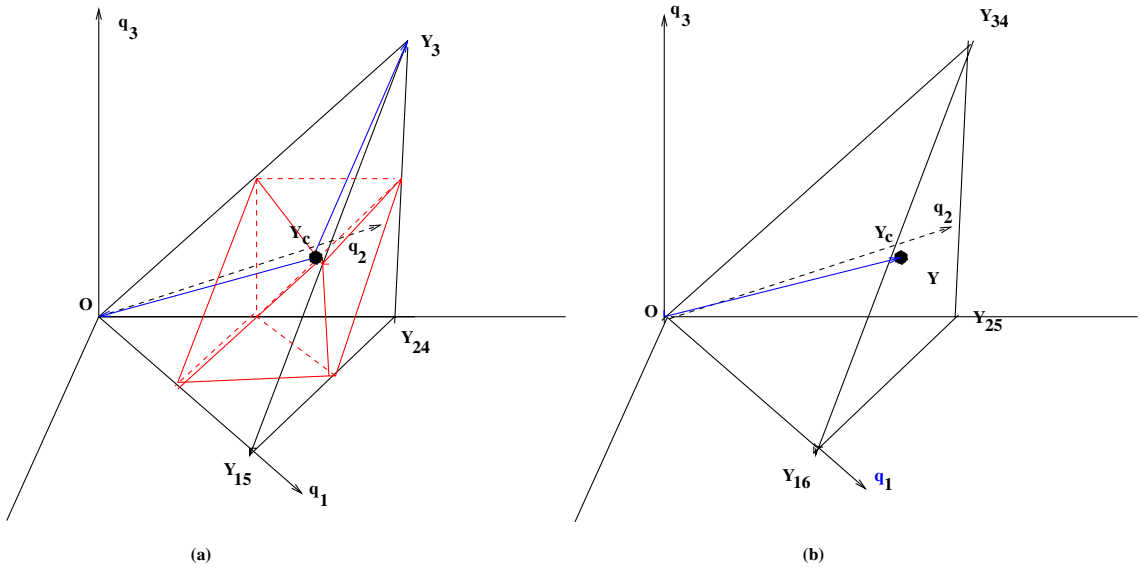

FIG. 16 (color online). The three-dimensional subspaces where the Polyakov loop is real: left for six colors and right for seven. The planes where $\mathrm{tr}\mathbf{L}^n$ vanish are given in the left panel.

Fig. 12. Now the path from the perturbative vacuum to the confined vacuum is not a straight line, $\mathbf{OY}_c$, but slightly bent. This is irrelevant, though: the point is that if we expand any effective potential about $\mathbf{Y}_c$, simply from the shape of the Weyl chamber, it is clearly not symmetric. Thus, we expect the expansion of an effective potential, about $\mathbf{Y}_c$, to reflect the lack of such symmetry. This is the reason for the cubic terms in Eq. (136).

The same argument applies for higher N. When $N = 2M$, the part of the Weyl chamber in which the Polyakov loop is real is M dimensional, and so it becomes more difficult to draw. Even so, the lack of symmetry about the confined vacuum for six colors can also be seen from Fig. 16.

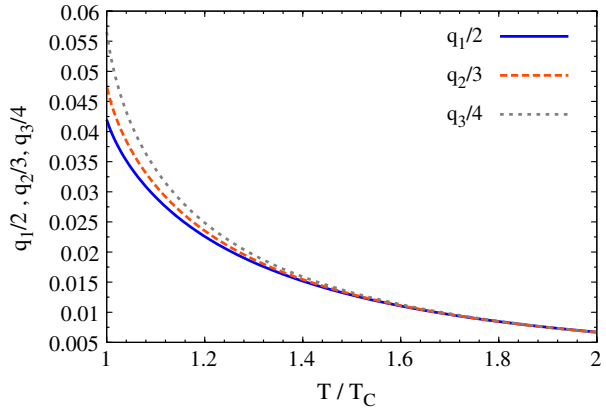

FIG. 17 (color online). The numerical solution for seven colors, with $c_2 = 0.23$. The deviation from $q_1/2 = q_2/3 = q_3/4$ indicates the deviation from the uniform eigenvalue ansatz.

VIII. A $G(2)$ GAUGE GROUP AND THE LAW OF MAXIMAL EIGENVALUE REPULSION

A. Motivation

For $SU(N)$ groups the Polyakov loop vanishes below T_c and there is a strict definition of the deconfining transition temperature. That the Polyakov loop vanishes is a consequence of the center of $SU(N)$ and the associated global $Z(N)$ symmetry. The confined vacuum, $\mathbf{Y}_c$, is also the point where there is maximal repulsion of the eigenvalues, Eq. (44). We shall see in this section that it may be more useful to think of confinement as arising not from the center symmetry *per se* but from eigenvalue repulsion.

To this end, we consider groups without a center. Such groups have been considered before, starting with $SO(3)$ [70–72]. The group $SO(3) = SU(2)/Z(2)$ and it has $SU(2)$ as a two-fold covering group. Consequently, the first homotopy group is nontrivial, $\Pi_1(SO(3)) = Z(2)$. This is true for all $SO(2N + 1)$ groups: they have a two-fold covering representation, $Spin(2N + 1)$, which has a center of $Z(2)$, and are doubly connected.

Like the odd dimensional rotation groups, $G(2)$ has a trivial center. Unlike $SO(2N + 1)$ groups, though, $G(2)$ is simply connected, and for this reason it is especially interesting to consider [36–38,69–72]. In fact, $G(2)$ is a subgroup of $SO(7)$. This means that the eight-dimensional spin representation of $SO(7)$ has no subgroup that corresponds to a two-fold covering of $G(2)$.

Because there is no center, in $SO(3)$ and $G(2)$ Polyakov loops in the fundamental representation can be screened dynamically. In $SO(3)$, two fundamentals screen each other, $\mathbf{3} \otimes \mathbf{3} = \mathbf{1} + \mathbf{3} + \mathbf{5}$. In $G(2)$, the fundamental $\mathbf{7}$ field

can be screened by three adjoint **14** fields, $\mathbf{14} \otimes \mathbf{14} \otimes \mathbf{14} = \mathbf{1} + \mathbf{7} + \ldots$. This is unlike $SU(N)$, where $Z(N)$ symmetry prevents the fundamental field from being screened. Thus the $SO(3)$ and $G(2)$ groups are similar to QCD with dynamical quarks. Consequently, one might expect that there is no deconfining phase transition but just a smooth crossover from low-to high-temperature phases.

Nevertheless, lattice simulations for the $G(2)$ group find strong evidence for a first-order transition [36–41]. Even more strikingly, the expectation value of the Polyakov loop in the fundamental representation appears to be *very* small in the low-temperature phase: to a good approximation, the low temperature phase *is* confining. We thus need to construct effective potentials that give confinement, and a deconfining phase transition, in the absence of any center symmetry.

The simplest approach was suggested following Eq. (18). For $SU(N)$, the perturbative potential is a power series in the adjoint loop. The $Z(N)$ symmetry allows arbitrary powers of the $Z(N)$ neutral adjoint loop to appear but forbids terms which are charged under $Z(N)$, such as odd powers of the fundamental loop. Since $G(2)$ has no center symmetry, though, in the nonperturbative potential there is nothing to prevent us from adding arbitrary powers of the fundamental loop in Eq. (18). If the coefficients of such terms are large and of the right sign, they drive the theory into the confined phase at low temperatures.

Another approach is to observe that $SU(7) \supset SO(7) \supset G(2)$. This implies that we can construct a nonperturbative potential from both $SU(7)$ and $G(2)$ potentials. Of course, we must restrict the $SU(7)$ potentials to the two-dimensional Cartan space of $G(2)$. An easy exercise shows the confining vacuum for $SU(7)$, $\mathbf{Y}_c(7)$, lies in the Cartan space of $G(2)$. Thus, by carefully adjusting the parameters of the potential, we can ensure that the system lies in the $SU(7)$ confining vacuum below T_c. Confinement in $SU(7)$ then drives the fundamental loop to vanish as well.

In both cases, we add terms to the nonperturbative potential which give an expectation value for the fundamental loop that is either small or zero in the low-temperature phase. Confinement is thus driven not by the center symmetry, but through the complete repulsion of eigenvalues.

The crucial question is whether the Weyl invariance of $G(2)$ is respected by such $SU(7)$ potentials. The following simple argument is suggestive. The Weyl group of $SU(7)$ is the permutation group S_7. The Weyl group of $SO(7)$ is O_h, the group of rotations and reflections that leave the three-dimensional cube invariant and is of order 48. The Weyl group of $G(2)$ is D_6, the dihedral group of order 12. Now the latter two can be written as semidirect products of S_2 with S_4 and S_3, respectively. This shows that they are subgroups of S_7. So, Weyl invariance is respected if one neglects the fact that S_7 acts in the six-dimensional Cartan space of $SU(7)$, whereas D_6 acts in the two-dimensional Cartan space of $G(2)$.

In Sec. VIII B we discuss the three-dimensional Cartan space of $SO(7)$, the embedded Cartan space of $G(2)$, and their roots. Section VIII C constructs confining potentials for both $G(2)$ and $SO(7)$. In Sec. VIII D we give a simple proof that the $SU(7)$-type potential respects the necessary Weyl symmetry. Finally, in Sec. VIII E we give results for the possible thermodynamic behavior of $G(2)$ on the basis of some possible models.

B. The root systems of $SU(7)$, $SO(7)$, and $G(2)$

We start with some basic facts and notation. The Polyakov loop for $SU(7)$ is $\mathbf{L} = \exp(2\pi i \mathbf{q}_{SU7})$, where

$$\mathbf{q}_{SU7} = \mathrm{diag}(q_1, q_2, q_3, q_4, q_5, q_6, q_7). \tag{137}$$

As an element of $SU(7)$, this is a traceless matrix,

$$q_1 + \cdots + q_7 = 0, \tag{138}$$

and defines the six-dimensional Cartan space of $SU(7)$.

The group $SU(7)$ has the subgroup $SO(7)$. The Cartan space of $SO(7)$ is three dimensional, where the q's obey three extra constraints,

$$q_7 = q_1 + q_4 = q_2 + q_5 = 0. \tag{139}$$

Note that these constraints are identical to those which ensure that the trace of the fundamental loop in $SU(7)$ is real, as illustrated in Fig. 16.

The group $G(2)$ is a subgroup of $SO(7)$. Its Cartan subspace obeys one more constraint:

$$q_1 + q_2 + q_3 = 0. \tag{140}$$

We write the corresponding matrix as $\mathbf{q}_{G2}$, which has two degrees of freedom.

In Fig. 18 we show the three-dimensional root system of $SO(7)$ and its $G(2)$ subgroup. Here the basis vector corresponding to (q_1, q_2, q_3) are $\vec{e}_{1,2,3}$. This figure also illustrated the restriction to the $G(2)$ plane, where $q_1 + q_2 + q_3 = 0$. From this figure and standard group theory [62], the roots are given by

$$\vec{\alpha}^{\pm}_{ij} = \vec{e}_i \pm \vec{e}_j, ; \qquad \vec{\beta}_i = \vec{e}_i, ; \qquad i\colon 1 \ldots 3, \tag{141}$$

together with the six roots with opposite sign.

The twelve roots $\vec{\alpha}^{\pm}$ lie on the edges of the cube, and the six roots $\vec{\beta}$ on the vertices of the octahedron. The Weyl group of this system is O_h, the group of rotations and reflections that leave the cube and the octahedron invariant, and is of order 48. The group of rotations is identical to the permutation group, S_4, of the four-diagonal body axes of the cube.

The plane defined by $q_1 + q_2 + q_3 = 0$ contains the six $SU(3)$-like roots $\vec{\alpha}^{-}_{ij}$:

$$\vec{\alpha}^{-}_{12} = \vec{e}_1 - \vec{e}_2; \qquad \vec{\alpha}^{-}_{23} = \vec{e}_2 - \vec{e}_3; \qquad \vec{\alpha}^{-}_{31} = \vec{e}_3 - \vec{e}_1. \tag{142}$$

These are part of the $SO(7)$ root system. Then there are the six orthogonal projections of the short roots $\vec{\beta}_i$ in $SO(7)$ onto the plane $q_1 + q_2 + q_3 = 0$. The resulting projections

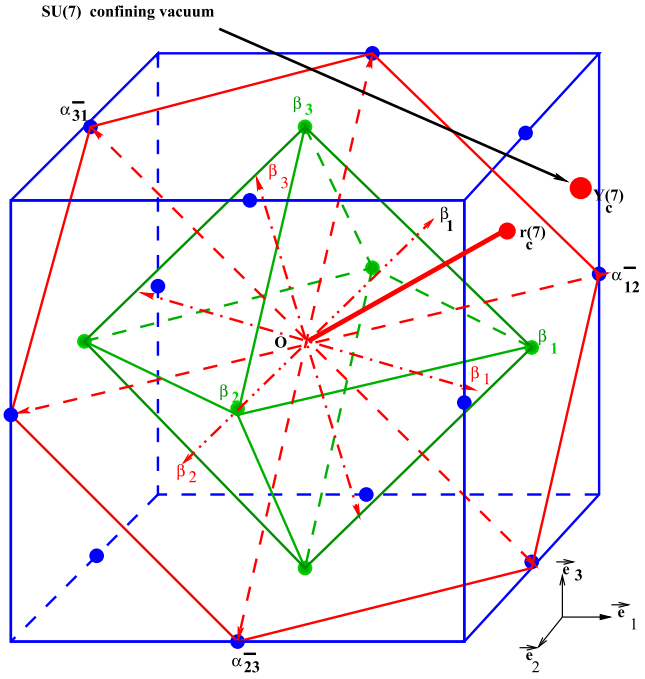

FIG. 18 (color online). The root system of $SO(7)$ and its $G(2)$ subgroup. Also shown are the confining $SU(7)$ vacuum, $\mathbf{Y}_c(7)$, and $r_c(7)$, the solution for the $SU(7)$ potential at T_c^+.

are denoted by β_i in Fig. 18. Below, we write them as $\hat{\vec{\beta}}_i$ to avoid confusion with the corresponding $SO(7)$ roots $\vec{\beta}_i = \vec{e}_i$:

$$\begin{aligned}\hat{\vec{\beta}}_1 &= \frac{1}{3\sqrt{2}}(2\vec{e}_1 - \vec{e}_2 - \vec{e}_3);\\ \hat{\vec{\beta}}_2 &= \frac{1}{3\sqrt{2}}(-\vec{e}_1 + 2\vec{e}_2 - \vec{e}_3);\\ \hat{\vec{\beta}}_2 &= \frac{1}{3\sqrt{2}}(-\vec{e}_1 - \vec{e}_2 + 2\vec{e}_3).\end{aligned} \tag{143}$$

The $\hat{\vec{\beta}}$ roots are indeed $1/\sqrt{3}$ shorter then the $SU(3)$-like roots $\vec{\alpha}^-$, as behooves the root system of $G(2)$. Note that the $SU(3)$ hypercharge matrices $\mathbf{Y}_1 \sim \mathrm{diag}(1, 1, -2)$ and their permutations are generating the $\hat{\beta}$ roots in the same way as the $SU(2)$ matrices $\mathrm{diag}(1, -1)$ generate the $\vec{\alpha}^-$ roots.

As in Eq. (32) we define

$$\mathbf{q}_{G2} = \vec{\mathbf{q}}_{G2} \cdot \vec{H}. \tag{144}$$

In the perturbative effective potential, Eq. (31), the short and long roots of $G(2)$ appear as $\hat{\vec{\beta}}_i \cdot \vec{\mathbf{q}}_{G2}$ and $\vec{\alpha}_{ij}^- \cdot \vec{\mathbf{q}}_{G2}$. These arguments are easily found from Eqs. (142) and (143). They are, with the condition $q_1 + q_2 + q_3 = 0$:

$$\begin{aligned}&\vec{\alpha}_{12}^- \cdot \vec{\mathbf{q}}_{G2} = q_1 - q_2;\\ &\vec{\alpha}_{23}^- \cdot \vec{\mathbf{q}}_{G2} = q_2 - q_3;\ \vec{\alpha}_{31}^- \cdot \vec{\mathbf{q}}_{G2} = q_3 - q_1.\end{aligned} \tag{145}$$

$$\hat{\vec{\beta}}_1 \cdot \vec{\mathbf{q}}_{G2} = q_1; \qquad \hat{\vec{\beta}}_2 \cdot \vec{\mathbf{q}}_{G2} = q_2; \qquad \hat{\vec{\beta}}_3 \cdot \vec{\mathbf{q}}_{G2} = q_3. \tag{146}$$

The root lattice of $G(2)$ and its Weyl chamber are illustrated in Fig. 19. The left panel is the root lattice, with six long and six short roots. The Weyl group is generated by the two mirrors indicated in the left panel, at an angle of $2\pi/12$. The product of the two reflections is a rotation over $2\pi/6$. The group is generated by this six-fold rotation and by one of the reflections. This gives the dihedral group of order 12, and so 12 Weyl chambers. These are shown in the right-hand panel. We pick the Weyl chamber as defined by the points **O**, and $(1, -2, 1)/3$, and $(1, -1, 0)/2$. This is the upper half of the Weyl chamber of $SU(3)$ in Fig. 2. We also indicate the confining vacuum for $SU(3)$, $\mathbf{Y}_c(3) = (1, -1, 0)/3$; the confining vacuum for $SU(7)$, $\mathbf{Y}_c(7) = (2, -3, 1)/7$, and by a black curve, the path where trace of the fundamental

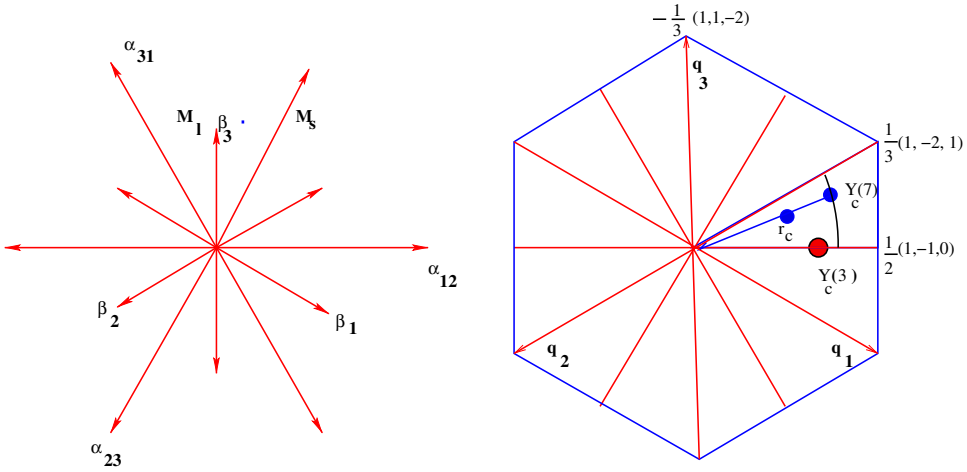

FIG. 19 (color online). Left: the root lattice of $G(2)$. Right: the twelve Weyl chambers of $G(2)$. $\mathbf{Y}_c(3)$ is the $SU(3)$ confined vacuum; $\mathbf{Y}_c(7)$, that for $SU(7)$.

loop in $G(2)$ vanishes. The Weyl chamber for $G(2)$ is precisely half that of $SU(3)$, Fig. 2.

C. Confining potentials for $G(2)$ and $SO(7)$

We drop an overall factor of T^4 from the potential and split it into perturbative and nonperturbative parts,

$$V_{\rm tot}(\mathbf{q}_{G2}) = V_{\rm pt}^{G(2)}(\mathbf{q}_{G2}) + V_{\rm np}(\mathbf{q}_{G2}). \tag{147}$$

As discussed in Sec. III the perturbative $G(2)$ potential is

$$V_{\rm pt}^{G(2)}(\mathbf{q}_{G2}) = -\frac{14}{45}\pi^2 + \frac{4\pi^2}{3}V_2^{G(2)}(\mathbf{q}_{G2}), \tag{148}$$

where $t = T/T_c$, and

$$2V_k^{G(2)}(\mathbf{q}_{G2}) = \sum_\alpha B_{2k}(\vec{\alpha}\cdot\vec{\mathbf{q}}_{G2}) + \sum_\beta B_{2k}(\vec{\beta}\cdot\vec{\mathbf{q}}_{G2}), \quad k = 1, 2, \tag{149}$$

with the roots α and β those of $G(2)$.

We now consider the types of nonperturbative potentials that can produce a confined phase at low temperature. Certainly we can add terms $\sim V_k^{G(2)}(\mathbf{q}_{G2})$, as we did for $SU(N)$. Generically, though, these do not give low-temperature phases that are confining.

The first method is to take a sum as in Eq. (18), but sum over powers of the Wilson line in the fundamental representation, the **7**. The weights of the **7** are precisely the six $\pm\vec{\hat{\beta}}_i$, $i = 1, 2, 3$ from Eq. (146). This gives a potential

$$V_2^7(\mathbf{q}_{G2}) = B_4(q_1) + B_4(q_2) + B_4(q_3). \tag{150}$$

The second method is to add potentials from $SU(7)$. This will give terms $V_k^{SU(7)}(\mathbf{q}_{G2})$, where these potentials are defined by summing the corresponding Bernoulli polynomials B_{2k} over the roots $\vec{\alpha}_{ij}^-$, $1 \le i < j \le 7$ of $SU(7)$:

$$V_k^{SU(7)}(\mathbf{q}_{G2}) = \sum_{1\le i<j\le 7} B_{2k}(\vec{\alpha}_{ij}^-\cdot\vec{\mathbf{q}}_{G2}). \tag{151}$$

By appropriately adjusting the coefficients in the nonperturbative potential, we show that we can ensure that at the critical temperature, the system goes into the $SU(7)$-confining confining vacuum $Y_c(7)$. We stress there is no elegance in our approach: we are manifestly constructing a confined vacuum by hand. Nevertheless, our model gives testable predictions, as shown in Sec. VIII E.

Along these same lines we can also construct a potential that generates confinement in $SO(7)$: the perturbative potential is that for $SO(7)$, while in the $SU(7)$-like potential, Eq. (151), we change the argument to $\mathbf{q}_{SO(7)}$. Doing this gives:

$$V_{\rm tot}(\mathbf{q}_{SO(7)}) = V_{\rm pt}^{SO(7)}(\mathbf{q}_{SO(7)}) + V_{np}(\mathbf{q}_{SO(7)}), \tag{152}$$

where

$$V_{\rm pt}^{SO(7)}(\mathbf{q}_{SO(7)}) = -\frac{21}{45}\pi^2 + \frac{4\pi^2}{3}V_2^{SO(7)}(\mathbf{q}_{SO(7)}), \tag{153}$$

and

$$2V_k^{SO(7)}(\mathbf{q}_{SO(7)}) = \sum_\alpha B_{2k}(\vec{\alpha}\cdot\vec{\mathbf{q}}_{SO(7)}) + \sum_\beta B_{2k}(\vec{\beta}\cdot\vec{\mathbf{q}}_{SO(7)}), \quad k = 1, 2, \tag{154}$$

with the roots α and β those of $SO(7)$. The $SU(7)$-like potentials are

$$V_k^{SU(7)}(\mathbf{q}_{SO(7)}) = \sum_{1\le i<j\le 7} B_{2k}(\vec{\alpha}_{ij}^-\cdot\vec{\mathbf{q}}_{SO(7)}). \tag{155}$$

As discussed following Eq. (35), perturbatively the $\mathbf{q}$ potentials for $SO(7)$ and $Sp(6)$ are related by duality. If one generates maximal eigenvalue repulsion for $Sp(6)$, however, one obtains confinement appropriate to $SU(6)$, while Eq. (155) for $SO(7)$ gives confinement like that of $SU(7)$. If the law of maximal eigenvalue repulsion holds, then the nonperturbative potentials are not related by duality [58].

D. Weyl symmetry of $SU(7)$-like potentials

In this subsection we show that the nonperturbative potentials introduced above are invariant under the Weyl symmetries of $G(2)$ and $SO(7)$. First, observe that the only terms which are not manifestly Weyl invariant are those in Eqs. (151) and (155).

In the case of $G(2)$ we use Eq. (32) to write the potential as:

$$\begin{aligned} V_k^{SU(7)}(\mathbf{q}_{G2}) &= \frac{1}{2}\sum_{1\le i,j\le N} B_2(q_i - q_j) \\ &= 2(B_{2k}(q_1-q_2) + B_{2k}(q_2-q_3) + B_{2k}(q_3-q_1)) \\ &\quad + 4(B_{2k}(q_1) + B_{2k}(q_2) + B_{2k}(q_3)) + B_{2k}(2q_1) \\ &\quad + B_{2k}(2q_2) + B_{2k}(2q_3), \end{aligned} \tag{156}$$

with $q_1 + q_2 + q_3 = 0$.

Now, use Eq. (146) to rewrite this in terms of the roots of $G(2)$ roots. This gives:

$$2V_k^{SU(7)}(\mathbf{q}_{G2}) = 4\sum_\alpha B_{2k}(\vec{\alpha}\cdot\vec{\mathbf{q}}_{G2}) + \sum_\beta (2B_{2k}(\vec{\beta}\cdot\vec{\mathbf{q}}_{G2}) + B_{2k}(2\vec{\beta}\cdot\vec{\mathbf{q}}_{G2})), \tag{157}$$

which is manifestly invariant under the Weyl symmetry of $G(2)$.

Applying the same method to $SO(7)$ gives

$$V_k^{SU(7)}(\mathbf{q}_{SO(7)}) = B_{2k}(2q_1) + B_{2k}(2q_2) + B_{2k}(2q_3) + 2(B_{2k}(q_1) + B_{2k}(q_2) + B_{2k}(q_3)) + 2(B_{2k}(q_1 - q_2) + B_{2k}(q_2 - q_3) + B_{2k}(q_3 - q_1) + B_{2k}(q_1 + q_2) + B_{2k}(q_2 + q_3) + B_{2k}(q_3 + q_1)). \quad (158)$$

Note that the constraint $q_1 + q_2 + q_3 = 0$ is absent for $SO(7)$. Imposing it gives the $G(2)$ result, Eq. (156). Using Eqs. (33) and (34), this can be rewritten as

$$2V_k^{SU(7)}(\mathbf{q}_{SO(7)}) = 2\sum_\alpha B_{2k}(\vec{\alpha}\cdot\vec{\mathbf{q}}_{SO(7)}) + \sum_\beta (2B_{2k}(\vec{\beta}\cdot\vec{\mathbf{q}}_{SO(7)}) + B_{2k}(2\vec{\beta}\cdot\vec{\mathbf{q}}_{SO(7)})). \quad (159)$$

This result is manifestly Weyl invariant as the sums are separately invariant: the Weyl transformations are orthogonal and so cannot transform α roots into β roots.

E. Results for $G(2)$

In this section, we give results for the thermodynamics, assuming parameters which give a confined low-temperature phase. The total potential is

$$\mathcal{V}_{\text{tot}}^{\text{G(2)}}(\mathbf{q}_{G2}) = T^4(V_{\text{pt}}^{\text{G(2)}}(\mathbf{q}_{G2}) + V_{\text{npt}}(\mathbf{q}_{G2}, t)), \quad (160)$$

where the perturbative potential is

$$V_{\text{pt}}^{\text{G(2)}}(\mathbf{q}_{G2}) = -\frac{14\pi^2}{45} + \frac{4\pi^2}{3}V_2^{\text{G(2)}}(\mathbf{q}_{G2}). \quad (161)$$

For clarity, we write all functions in terms of the two independent q's for $G(2)$, q_1 and q_2. The $G(2)$ potentials are

$$V_n^{\text{G(2)}}(\mathbf{q}_{G2}) = B_{2n}(q_1) + B_{2n}(q_2) + B_{2n}(q_1 + q_2) + B_{2n}(q_1 - q_2) + B_{2n}(2q_1 + q_2) + B_{2n}(q_1 + 2q_2). \quad (162)$$

We consider a nonperturbative potential

$$V_{\text{np}}(\mathbf{q}_{G2}) = -\frac{4\pi^2}{3t^2}(c_1^{G(2)}V_1^{G(2)}(\mathbf{q}_{G2}) + c_1^{SU(7)}V_1^{SU(7)}(\mathbf{q}_{G2}) + c_2^{G(2)}V_2^{G(2)}(\mathbf{q}_{G2}) + c_2^{SU(7)}V_2^{SU(7)}(\mathbf{q}_{G2}) + d_2^{G(2)}V_2^{\mathbf{7}}(\mathbf{q}_{G2}) + c_3). \quad (163)$$

The $SU(7)$ potentials are

$$V_n^{SU(7)}(q_1, q_2) = B_{2n}(2q_1) + B_{2n}(2q_2) + B_{2n}(2q_1 + 2q_2) + 2(B_{2n}(q_1 - q_2) + B_{2n}(2q_1 + q_2) + B_{2n}(q_1 + 2q_2)) + 4(B_{2n}(q_1) + B_{2n}(q_2) + B_{2n}(q_1 + q_2)), \quad (164)$$

while the potential from summing over Eq. (18) using the fundamental representation, the **7**, is

$$V_2^{\mathbf{7}}(\mathbf{q}_{G2}) = B_4(q_1) + B_4(q_2) + B_4(q_1 + q_2). \quad (165)$$

Besides thermodynamic quantities, such as the pressure and the interaction measure, it is also possible to measure loops. In $G(2)$, the fundamental representation is related to the $SU(3)$ embedding as $\mathbf{7} = \mathbf{1} + \mathbf{3} + \bar{\mathbf{3}}$ [36], so that the fundamental loop is given by [40]

$$\ell_{\mathbf{7}} = \frac{1}{7}(1 + 2\cos(2\pi q_1) + 2\cos(2\pi q_1) + 2\cos(2\pi(q_1 + q_2))). \quad (166)$$

The adjoint representation is related to the $SU(3)$ embedding as $\mathbf{14} = \mathbf{3} + \bar{\mathbf{3}} + \mathbf{8}$, so that [40]

$$\ell_{\mathbf{14}} = \frac{1}{7}(1 + \cos(2\pi q_1) + \cos(2\pi q_1) + \cos(2\pi(q_1 + q_2)) + \cos(2\pi(q_1 - q_2)) + \cos(2\pi(2q_1 + q_2)) + \cos(2\pi(q_1 + 2q_2)). \quad (167)$$

In Eq. (163) we have a model with six parameters. Even imposing two conditions—that the transition occur at T_c and that the pressure vanishes there—we are left with four free parameters. Instead of investigating the entire four-dimensional space, we consider the behavior in some representative models.

The first is a minimal $G(2)$ model,

$$c_1^{G(2)}, \quad c_3 \neq 0; \quad c_2^{G(2)} = c_1^{SU(7)} = c_2^{SU(7)} = d_2^{G(2)} = 0. \quad (168)$$

This is the $G(2)$ analogy of the analogue of the zero-parameter $SU(N)$ model of Ref. [20]. We introduce terms $\sim c_1^{G(2)}B_2(\mathbf{q}_{G2})$ to drive the theory to a Higgs phase. We could also introduce a term $\sim c_2^{G(2)}B_4(\mathbf{q}_{G2})$, which would be like our one parameter $SU(N)$ model [14]. We have done so and find that the results are similar to the minimal model of Eq. (168).

The next is a model with a single fundamental loop,

$$d_2^{G(2)}, \quad c_1^{G(2)}, \quad c_2^{G(2)}, \quad c_3 \neq 0; \quad c_1^{SU(7)} = c_2^{SU(7)} = 0. \quad (169)$$

The specific parameters chosen were $d_2^{G(2)} = -0.210$ and $c_2^{G(2)} = 0.3$; the values of $c_1^{G(2)}$ and c_3 follow as for $SU(N)$, Sec. IV, and are $c_1^{G(2)} = 0.278$ and $c_3 = -0.364$.

Finally, we consider a $SU(7)$-type model,

$$c_2^{G(2)} = 1; \quad c_1^{SU(7)}, \quad c_2^{SU(7)}, \quad c_3 \neq 0; \quad c_1^{G(2)} = d_2^{G(2)} = 0. \tag{170}$$

Notice that we have fixed the parameter $c_2^{G(2)} = 1$; with this value, the $G(2)$ part of the nonperturbative potential cancels, *identically*, the perturbative $G(2)$ potential at T_c. This ensures that the confining effects of the $SU(7)$ potential are maximized at T_c. We then considered two representative values of $c_2^{SU(7)}$: $c_2^{SU(7)} = 2.0$, for which $c_1^{SU(7)} = 0.623$, and $c_3 = -1.093$; and $c_2^{SU(7)} = 4.0$, for which $c_1^{SU(7)} = 1.246$ and $c_3 = -1.952$.

In Fig. 20 we show the expectation value of the Polyakov loops in the fundamental representations. At present, there is only data on histograms for the expectation value for the bare, fundamental loop [36–41]. This shows the expectation value of the bare loop is very small in the low-temperature phase. Including renormalization should not alter this conclusion. Presumably, more careful lattice studies will show that the expectation value is small, but nonzero, as is true for the adjoint loop in $SU(3)$ below T_c [31].

Nevertheless, the minimal $G(2)$ model appears to be excluded. The fundamental loop is negative at T_c^-, with a value ~ -0.2. In Fig. 21 we illustrate the Weyl chamber for $G(2)$, indicating both the vacua at T_c^+ and T_c^-. The low-temperature phase at T_c^- is close but not coincident with $\mathbf{Y}_c(7)$, the confining vacuum for $SU(7)$.

The other models give fundamental loops which are small in the low-temperature phase. In the fundamental loop model, this expectation value is $\sim +0.05$ at T_c^-, which may be compatible with the lattice results. Lastly, the $SU(7)$ models automatically give zero fundamental loop below T_c.

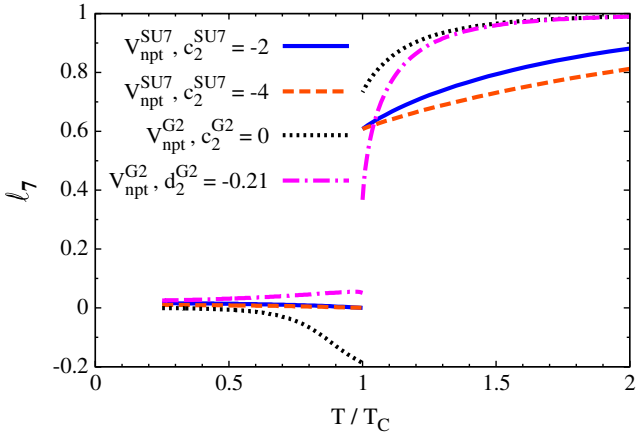

FIG. 20 (color online). Expectation value of the Polyakov loop in the fundamental representation of $G(2)$ for the minimal $G(2)$ model, Eq. (168); the fundamental loop model, Eq. (169); and the two $SU(7)$ models, Eq. (170).

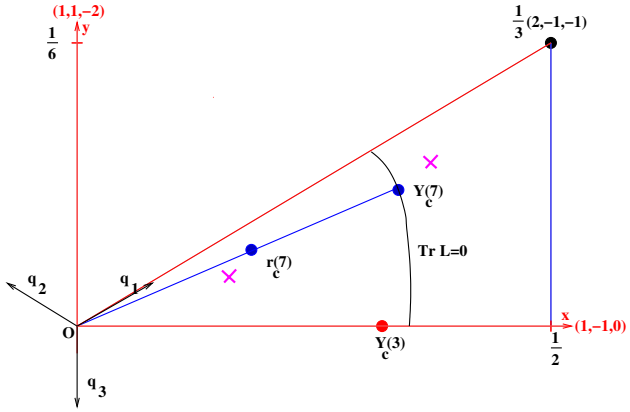

FIG. 21 (color online). Trajectories in the Weyl chamber of $G(2)$, Fig. 19. The crosses denote the vacua at $T_c^{\pm}$ for the minimal $G(2)$ model; $\mathbf{Y}_c(7)$ is the confining $SU(7)$ vacuum.

In Fig. 22 we give the expectation value of the adjoint loop. This also provides a way of distinguishing between different models. On the lattice, the bare adjoint loop is strongly suppressed but with effort can be measured. In the minimal $G(2)$ model, it is positive at T_c^-, but then becomes negative. It is negative in the low-temperature phase for the fundamental loop model and zero in the $SU(7)$ model.

Figure 23 shows the evolution of the eigenvalues of the fundamental Polyakov loop with temperature for the minimal $G(2)$ model, Eq. (168), and for the $SU(7)$ model, Eq. (169), with $c_2^{SU(7)} = -2$. We find that they remain close to, although not exactly on, the SU(7) path $|q_1/q_2| = 2$.

In Fig. 24 we show the pressure obtained from the four $G(2)$ models, Eqs. (168)–(170). This shows that the pressure itself is not very useful for differentiating between models. The pressure of the minimal $G(2)$ model is negative below T_c, but this is a limitation of our assumption that the pressure vanishes at T_c.

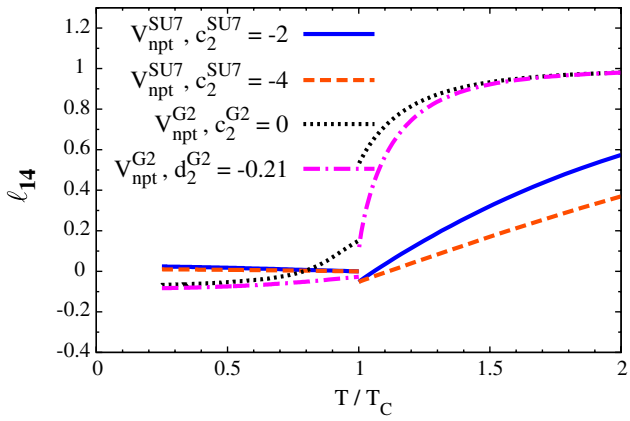

FIG. 22 (color online). Expectation value of the Polyakov loop in the adjoint representation of $G(2)$ for the minimal $G(2)$ model, Eq. (168); the fundamental loop model, Eq. (169); and two $SU(7)$ models, Eq. (170).

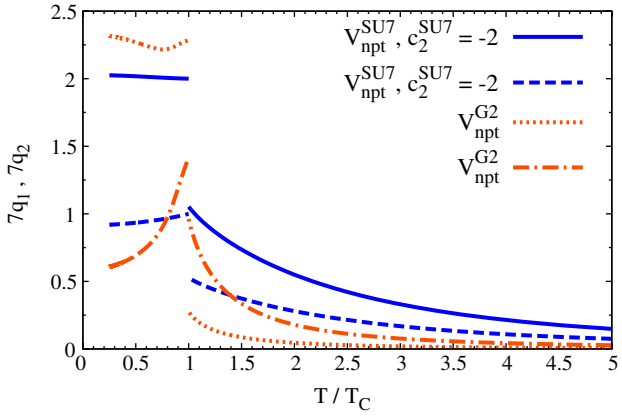

FIG. 23 (color online). Eigenvalues of the Polyakov loop for the minimal $G(2)$ model (dotted and dashed-dotted lines) and for one $SU(7)$ model (solid and dashed lines).

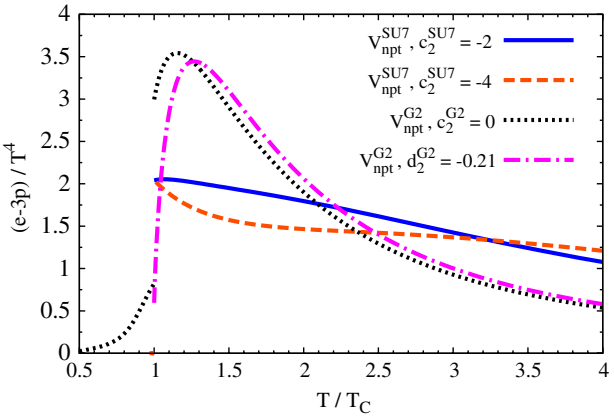

FIG. 25 (color online). Interaction measure, $(e - 3p)/T^4$, for our four $G(2)$ models.

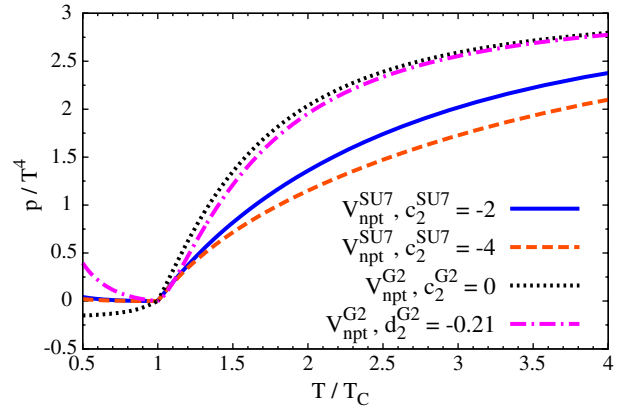

FIG. 24 (color online). Pressure for our four $G(2)$ models.

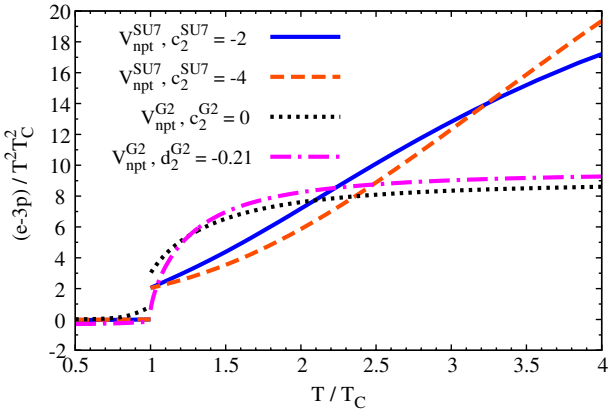

FIG. 26 (color online). Rescaled interaction measure, $(e - 3p)/T^2T_c^2$, for our four $G(2)$ models.

In Fig. 25 we show the interaction measure $(e - 3p)/T^4$ obtained from the $G(2)$ models. All of the transitions are of first order. The minimal $G(2)$ model looks most like that of $SU(N)$, with a large latent heat and a sharp peak in $(e - 3p)/T^4$ near T_c. The fundamental loop model also has a sharp peak in $(e - 3p)/T^4$, but its latent heat is small. Notice also that for the fundamental loop model, the expectation of the fundamental and adjoint loops, Figs. 20 and 22, is much smaller than the other models. This suggests that the fundamental loop model may be near a critical endpoint.

For the two $SU(7)$ models, the interaction measure $(e - 3p)/T^4$ does not exhibit a peak near T_c, but instead drops rather slowly as the temperature increases.

Lastly, in Fig. 26 we show the rescaled interaction measure, $(e - 3p)/T^2T_c^2$, for the four different models. For the minimal $G(2)$ and the fundamental loop models it is flat, while for the $SU(7)$ model it is not.

We await the results of more detailed numerical simulations in a lattice [41], which will enable us to fix the parameters of our effective model, Eq. (163).

IX. CONCLUSIONS

In this paper we generalized the model of Refs. [14,20] to a theory with two parameters. Their values were chosen by comparing to the interaction measure. We then obtain results for the 't Hooft loop above T_c and for the order-disorder interface tension at T_c. For most quantities the agreement is good, within 10% or so.

There is one glaring problem with the model: the results for the Polyakov loop, Figs. 3 and 8, look nothing like the lattice results, Refs. [31,32]. The discrepancy is not minor: on the lattice, the renormalized loop indicates a broad semi-QGP, from T_c to at least $3T_c$. In our model, the width is extremely narrow, to only $1.2T_c$. Further, the lattice measurements of Ref. [32] compute the renormalized loop by explicit subtraction of the zero-point energy at zero temperature, which is theoretically an unambiguous procedure.

Can corrections to our model change this? These are of two types. One is corrections in the coupling constant.

For example, there are corrections to $\sim g^2$ to the perturbative potential. It is also possible to compute corrections $\sim g^2$ to our potential, which includes both perturbative and nonperturbative terms [67]. (We ignore obvious questions of principle, namely, to what extent does the nonperturbative potential include perturbative corrections?) At next-to-leading order, it is known that the $\mathbf{q}$'s shift by an amount $\sim g^2$, [56], and the same happens in our effective model [67]. Such a shift is $\sim g^2$ and should be relatively small. More to the point, however, in our model the width of the transition region in the $\mathbf{q}$'s is tied intimately to the width of the interaction measure, and it seems unavoidable that a broad width in the $\mathbf{q}$'s gives a broad peak in the interaction measure.

Other corrections are those $\sim 1/N$. From lattice measurements, though, the behavior found for three colors [31] is very similar for four and five colors [32]. While the value of the Polyakov loop at the critical temperature changes modestly with N, in all cases the transition region, as seen from the renormalized Polyakov loop, remains broad.

This discrepancy must be considered the outstanding problem in the model. We can only suggest that the renormalized Polyakov loop does not directly reflect changes in the eigenvalue distribution of the Wilson line. For three [31,73] and four or five colors [32], there are terms $\sim 1/T^2$ in the logarithm of the Polyakov loop. It is conceivable that a nonperturbative mechanism broadens the (renormalized) Polyakov loop but not the distribution for the eigenvalues of the Wilson line. We suggest directly measuring how the distribution of the eigenvalues of the Wilson line changes with temperature [33,34].

We conclude by pointing out that there are two others ways in which the width of the transition region can be measured, although indirectly. One was discussed previously [14]. When the $\mathbf{q}$'s develop an expectation value, the theory is an adjoint Higgs phase. In our model, in principle this happens for all T, but in practice it is only numerically large below $1.2T_c$. While there is no order parameter to distinguish such an adjoint Higgs phase, it generates a characteristic splitting of masses. One may have to work very close to T_c to see this, but it is a necessary consequence of our model.

The 't Hooft loop provides another way of testing a narrow transition region. In Sec. V we gave results for the 't Hooft loop in the semi-QGP. Better measurements of these quantities should provide a stringent test of our model.

For four or more colors, there are further tests. For four colors, besides the simplest 't Hooft loop, between a Polyakov loop with phase 1 and i, there is also a loop between 1 and -1. To $\sim g^3$, the ratio of these 't Hooft loops satisfies Casimir scaling [57]. This Casimir scaling is observed to a very good precision over a wide range in temperature [66]. We have not computed the ratio of these 't Hooft loops in our model, but suggest that it will produce small but measurable deviations from Casimir scaling in the ratio of such 't Hooft loops when $T < 1.2T_c$.

In conclusion, we suggest that detailed measurements of the pure glue theory, especially near T_c, can help illuminate how the law of maximal eigenvalue repulsion acts to generate confinement.

ACKNOWLEDGMENTS

The research of A. D. was supported by the U.S. Department of Energy under Contract No. DE-FG02-09ER41620 and by PSC-CUNY Research Grant No. 64132-00 42; of Y. G. by a Grant from the NSFC of China with Project No. 11205035; of Y. H. by a Grant-in-Aid for Scientific Research (No. 23340067) from the Ministry of Education, Culture, Sports, Science and Technology (MEXT) of Japan; of R. D. P., by the U.S. Department of Energy under Contract No. DE-AC02-98CH10886. C. P. K. A. thanks the Nuclear Theory Group at BNL for their warm hospitality. We thank T. Umeda and the WHOT Collaboration for sharing their data with us [6], which enabled us to plot Fig. 1. R. D. P. thanks J. Pawlowski for numerous discussions on the model of Ref. [43], which also exhibits a narrow transition region; V. Begun, for bringing [23] to his attention; and A. Bazavov, F. Karsch, M. Panero, and P. Petreczky for discussions. C. P. K. A. thanks Oleg Ogievetsky and Loic Poulain d'Andecy for their explanations about classical groups.

[1] C. DeTar and U. Heller, Eur. Phys. J. A **41**, 405 (2009).
[2] P. Petreczky, J. Phys. G **39**, 093002 (2012).
[3] J. Engels, J. Fingberg, K. Redlich, H. Satz, and M. Weber, Z. Phys. C **42**, 341 (1989); J. Engels, J. Fingberg, and M. Weber, Nucl. Phys. **B332**, 737 (1990); J. Engels, J. Fingberg, and D. Miller, *ibid.* **B387**, 501 (1992); J. Engels, F. Karsch, and K. Redlich, *ibid.* **B435**, 295 (1995); J. Engels and T. Scheideler, *ibid.* **B539**, 557 (1999).
[4] G. Boyd, J. Fingberg, F. Karsch, L. Karkkainen, and B. Petersson, Nucl. Phys. **B376**, 199 (1992).
[5] B. Beinlich, F. Karsch, and A. Peikert, Phys. Lett. B **390**, 268 (1997).
[6] T. Umeda, S. Ejiri, S. Aoki, T. Hatsuda, K. Kanaya, Y. Maezawa, and H. Ohno, Phys. Rev. D **79**, 051501 (2009).
[7] S. Borsanyi, G. Endrodi, Z. Fodor, S. Katz, and K. Szabo, J. High Energy Phys. 07 (2012) 056.

[8] B. Lucini, M. Teper, and U. Wenger, J. High Energy Phys. 01 (2004) 061.
[9] B. Lucini, M. Teper, and U. Wenger, J. High Energy Phys. 02 (2005) 033.
[10] M. Teper, Proc. Sci., LATTICE2008 (2008) 022.
[11] M. Panero, Phys. Rev. Lett. **103**, 232001 (2009).
[12] S. Datta and S. Gupta, Phys. Rev. D **82**, 114505 (2010).
[13] B. Lucini, A. Rago, and E. Rinaldi, Phys. Lett. B **712**, 279 (2012).
[14] A. Dumitru, Y. Guo, Y. Hidaka, C. P. Korthals Altes, and R. D. Pisarski, Phys. Rev. D **83**, 034022 (2011).
[15] Y. Hidaka and R. D. Pisarski, Phys. Rev. D **78**, 071501 (2008); **80**, 036004 (2009); **80**, 074504 (2009); **81**, 076002 (2010).
[16] R. D. Pisarski, Phys. Rev. D **62**, 111501 (2000).
[17] A. Dumitru, Y. Hatta, J. Lenaghan, K. Orginos, and R. D. Pisarski, Phys. Rev. D **70**, 034511 (2004).
[18] A. Dumitru, J. Lenaghan, and R. D. Pisarski, Phys. Rev. D **71**, 074004 (2005).
[19] M. Oswald and R. D. Pisarski, Phys. Rev. D **74**, 045029 (2006).
[20] P. N. Meisinger, T. R. Miller, and M. C. Ogilvie, Phys. Rev. D **65**, 034009 (2002); P. N. Meisinger and M. C. Ogilvie, Phys. Rev. D **65**, 056013 (2002).
[21] R. D. Pisarski, Phys. Rev. D **74**, 121703 (2006).
[22] O. Andreev, Phys. Rev. D **76**, 087702 (2007); Phys. Lett. B **659**, 416 (2008); Phys. Rev. Lett. **102**, 212001 (2009); Int. J. Mod. Phys. E **20**, 2189 (2011).
[23] V. Begun, M. Gorenstein, and O. Mogilevsky, Int. J. Mod. Phys. E **20**, 1805 (2011).
[24] J. M. Cornwall, J. Papavassiliou, and D. Binosi, *The Pinch Technique and Its Applications to Non-Abelian Gauge Theories* (Cambridge University Press, Cambridge, England, 2011).
[25] A. Peshier, B. Kampfer, O. Pavlenko, and G. Soff, Phys. Rev. D **54**, 2399 (1996); A. Peshier and W. Cassing, Phys. Rev. Lett. **94**, 172301 (2005).
[26] W. Cassing, Nucl. Phys. **A791**, 365 (2007); **A795**, 70 (2007); W. Cassing and E. Bratkovskaya, Nucl. Phys. **A831**, 215 (2009); E. Bratkovskaya, W. Cassing, V. Konchakovski, and O. Linnyk, Nucl. Phys. **A856**, 162 (2011); V. Ozvenchuk, O. Linnyk, M. Gorenstein, E. Bratkovskaya, and W. Cassing, arXiv:1203.4734.
[27] P. Castorina, D. E. Miller, and H. Satz, Eur. Phys. J. C **71**, 1673 (2011).
[28] M. Ruggieri, P. Alba, P. Castorina, S. Plumari, C. Ratti, and V. Greco, Phys. Rev. D **86**, 054007 (2012).
[29] M. Caselle, L. Castagnini, A. Feo, F. Gliozzi, and M. Panero, J. High Energy Phys. 06 (2011) 142.
[30] M. Caselle, L. Castagnini, A. Feo, F. Gliozzi, U. Gürsoy, M. Panero, and A. Schäfer, J. High Energy Phys. 05 (2012) 135.
[31] S. Gupta, K. Huebner, and O. Kaczmarek, Phys. Rev. D **77**, 034503 (2008).
[32] A. Mykkanen, M. Panero, and K. Rummukainen, J. High Energy Phys. 05 (2012) 069.
[33] A. Dumitru and D. Smith, Phys. Rev. D **77**, 094022 (2008); D. Smith, Phys. Rev. D **82**, 034503 (2010).
[34] D. Diakonov, C. Gattringer, and H.-P. Schadler, J. High Energy Phys. 08 (2012) 128.
[35] B. Svetitsky and L. G. Yaffe, Nucl. Phys. **B210**, 423 (1982).
[36] K. Holland, P. Minkowski, M. Pepe, and U. Wiese, Nucl. Phys. B, Proc. Suppl. **119**, 652 (2003).
[37] M. Pepe and U.-J. Wiese, Nucl. Phys. **B768**, 21 (2007).
[38] G. Cossu, M. D'Elia, A. Di Giacomo, B. Lucini, and C. Pica, J. High Energy Phys. 10 (2007) 100.
[39] C. Hoyos-Badajoz, B. Lucini, and A. Naqvi, J. High Energy Phys. 04 (2008) 075.
[40] B. H. Wellegehausen, A. Wipf, and C. Wozar, Phys. Rev. D **80**, 065028 (2009); **83**, 016001 (2011); **83**, 114502 (2011).
[41] M. Bruno, M. Caselle, M. Panero, and R. Pellegrini (unpublished).
[42] A. Vuorinen and L. G. Yaffe, Phys. Rev. D **74**, 025011 (2006); P. de Forcrand, A. Kurkela, and A. Vuorinen, Phys. Rev. D **77**, 125014 (2008); T. Zhang, T. Brauner, A. Kurkela, and A. Vuorinen, J. High Energy Phys. 02 (2012) 139.
[43] J. Braun, H. Gies, and J. M. Pawlowski, Phys. Lett. B **684**, 262 (2010); F. Marhauser and J. M. Pawlowski, arXiv:0812.1144; J. Braun, A. Eichhorn, H. Gies, and J. M. Pawlowski, Eur. Phys. J. C **70**, 689 (2010).
[44] O. Scavenius, A. Dumitru, and J. Lenaghan, Phys. Rev. C **66**, 034903 (2002); K. Fukushima, Phys. Lett. B **591**, 277 (2004); T. Hell, S. Rossner, M. Cristoforetti, and W. Weise, Phys. Rev. D **81**, 074034 (2010); K. Fukushima and T. Hatsuda, Rep. Prog. Phys. **74**, 014001 (2011); F. Buisseret and G. Lacroix, Phys. Rev. D **85**, 016009 (2012); D. Horvatic, D. Blaschke, D. Klabucar, and O. Kaczmarek, Phys. Rev. D **84**, 016005 (2011); T. Hell, K. Kashiwa, and W. Weise, Phys. Rev. D **83**, 114008 (2011).
[45] B. Layek, A. P. Mishra, and A. M. Srivastava, Phys. Rev. D **71**, 074015 (2005).
[46] K. Kashiwa, R. D. Pisarski, and V. V. Skokov, Phys. Rev. D **85**, 114029 (2012).
[47] R. D. Pisarski and V. V. Skokov, Phys. Rev. D **86**, 081701 (R) (2012).
[48] C. Sasaki and K. Redlich, Phys. Rev. D **86**, 014007 (2012).
[49] J. Liao and E. Shuryak, Phys. Rev. C **75**, 054907 (2007); **77**, 064905 (2008); Phys. Rev. Lett. **101**, 162302 (2008); Phys. Rev. D **82**, 094007 (2010); Phys. Rev. Lett. **102**, 202302 (2009); arXiv:1206.3989; E. Shuryak and T. Sulejmanpasic, Phys. Rev. D **86**, 036001 (2012).
[50] D. Diakonov and M. Oswald, Phys. Rev. D **68**, 025012 (2003); **70**, 016006 (2004); **70**, 105016 (2004); D. Diakonov, N. Gromov, V. Petrov, and S. Slizovskiy, Phys. Rev. D **70**, 036003 (2004); D. Diakonov and N. Gromov, Phys. Rev. D **72**, 025003 (2005); D. Diakonov and V. Petrov, Phys. Rev. D **76**, 056001 (2007).
[51] D. Diakonov, Nucl. Phys. B, Proc. Suppl. **195**, 5 (2009); D. Diakonov and V. Petrov, AIP Conf. Proc. **1343**, 69 (2011).
[52] N. Fukui, K. Kondo, A. Shibata, and T. Shinohara, arXiv:1205.4976; Phys. Rev. D **86**, 065020 (2012).
[53] M. Unsal and L. G. Yaffe, Phys. Rev. D **78**, 065035 (2008).

[54] M. Unsal, Phys. Rev. D **80**, 065001 (2009); M. Shifman and M. Unsal, Phys. Rev. D **78**, 065004 (2008); M. Unsal, Phys. Rev. Lett. **102**, 182002 (2009); M. Shifman and M. Unsal, Phys. Rev. D **79**, 105010 (2009); Phys. Lett. B **681**, 491 (2009); E. Poppitz and M. Unsal, J. High Energy Phys. 01 (2010) 098; D. Simic and M. Unsal, Phys. Rev. D **85**, 105027 (2012); M. Unsal and L. G. Yaffe, J. High Energy Phys. 08 (2010) 030; E. Poppitz and M. Unsal, J. High Energy Phys. 07 (2011) 082.

[55] E. Poppitz, T. Schaefer, and M. Unsal, arXiv:1205.0290.

[56] T. Bhattacharya, A. Gocksch, C. P. Korthals Altes, and R. D. Pisarski, Phys. Rev. Lett. **66**, 998 (1991); Nucl. Phys. **B383**, 497 (1992).

[57] P. Giovannangeli and C. P. Korthals Altes, Nucl. Phys. **B721**, 1 (2005); **B721**, 25 (2005).

[58] C. P. Korthals Altes (unpublished).

[59] V. Belyaev, Phys. Lett. B **254**, 153 (1991).

[60] C. P. Korthals Altes, Nucl. Phys. **B420**, 637 (1994).

[61] I. S. Gradshteyn and I. M. Ryzhik, *Table of Integrals, Series, and Products* (Academic Press, New York, 1980).

[62] H. Georgi, *Lie Algebras in Particle Physics* (Westview Press, Boulder, 1999).

[63] C. Korthals-Altes, A. Kovner, and M. A. Stephanov, Phys. Lett. B **469**, 205 (1999); C. Korthals-Altes and A. Kovner, Phys. Rev. D **62**, 096008 (2000).

[64] P. de Forcrand and D. Noth, Phys. Rev. D **72**, 114501 (2005).

[65] P. de Forcrand, M. D'Elia, and M. Pepe, Phys. Rev. Lett. **86**, 1438 (2001).

[66] P. de Forcrand, B. Lucini, and D. Noth, Proc. Sci., LAT2005 (2005) 323.

[67] A. Dumitru, Y. Guo, N. Su, and C. P. Korthals Altes (unpublished).

[68] B. Lucini, M. Teper, and U. Wenger, Phys. Lett. B **545**, 197 (2002).

[69] K. Holland, M. Pepe, and U. Wiese, Nucl. Phys. **B694**, 35 (2004).

[70] K. Langfeld and H. Reinhardt, arXiv:hep-lat/0001009.

[71] P. de Forcrand and O. Jahn, Nucl. Phys. **B651**, 125 (2003).

[72] J. Greensite, K. Langfeld, S. Olejnik, H. Reinhardt, and T. Tok, Phys. Rev. D **75**, 034501 (2007).

[73] E. Megias, E. Ruiz Arriola, and L. Salcedo, Phys. Rev. D **75**, 105019 (2007).